Pergamon

Chemical Engineering Science, Vol. 50, No. 11, pp. 1707–1736, 1995

0009-2509/95 $9.50 + 0.00

0009-2509(95)00026-7

DYNAMIC ULTRAFILTRATION MODEL FOR CHARGED COLLOIDAL DISPERSIONS: A WIGNER–SEITZ CELL APPROACH

W. RICHARD BOWEN† and FRANK JENNER
Biochemical Engineering Group, Department of Chemical Engineering, University College of Swansea, University of Wales, Swansea, SA2 8PP, U.K.

(*Received* 21 *September* 1994; *accepted in revised form* 5 *January* 1995)

Abstract—A rigorous, dynamic mathematical model for predicting the rate of ultrafiltration of charged colloidal dispersions is developed. The model is based on sophisticated descriptions of the particle–particle interactions within filter cakes which are responsible for controlling permeation rates. Electrostatic (double layer) interactions are accounted for by means of a Wigner–Seitz cell approach, including a numerical solution of the non-linear Poisson–Boltzmann equation, which is known to give an excellent description of the configurational electrostatic interaction energy of particle assemblages. London–van der Waals forces are calculated using a computationally efficient means of approximating screened, retarded Lifshitz–Hamaker constants. Hydration forces are included by utilising mathematical expressions derived from the latest results obtained with surface-forces apparatus. Configurational entropy effects are calculated using an equation of state giving excellent agreement with molecular dynamic data. Electroviscous effects are also accounted for. These descriptions of particle–particle interactions in assemblages are used to develop an *a priori* model, with no adjustable parameters, that allows quantitative prediction of the rate of filtration of charged colloidal dispersions as a function of zeta-potential, particle composition (through the Hamaker constant), ionic strength, applied pressure, particle radius and membrane resistance. This is a dynamic model which takes into account the variation of local specific cake resistance as a function of both position in the cake and time. The predictions of the model are systematically investigated, showing the great importance of taking particle–particle interactions into account for ultrafiltration. A comparison with experimental filtration data for colloidal silica shows that the model is in excellent agreement with such data.

INTRODUCTION

Membrane separation technology is a novel and highly innovative process engineering operation. In recent years, membrane separation processes have found wide application as an alternative to conventional industrial separation methods such as distillation, centrifugation and extraction. One of the most widely used is membrane ultrafiltration, a pressure driven process which is capable of separating particles in the approximate size range 1–500 nm. That is, it is a process capable of separating colloids. These colloids may be inorganic, polymeric or biological (e.g. metal oxides, lattices or proteins).

The design and successful application of membrane separation processes in the process industry requires the development of quantitative predictive models, which relate material properties to separation performances. The factors controlling the performance of ultrafiltration have been extensively reviewed (Fane, 1986; Bowen and Jenner, 1995a). There have been a number of seminal approaches in this field. Most have been based on the rate limiting effects of the concentration polarisation of the separated colloids at the membrane surface. (In industrial practice, such concentration polarisation is controlled by flowing the process feed along the surface of the membrane at velocities in the range 1–8 $m\,s^{-1}$, a process termed "cross-flow" filtration). Such a consideration of concentration polarisation, taken in conjunction with the formation of a "gel" of dispersed materials beyond a critical high concentration, led to the formulation of the "gel-polarisation-film" model (Michaels, 1968). This model and recent sophistications allowing for variations in viscosity and diffusion coefficient across the concentration polarised boundary film have given a successful description for the ultrafiltration of some macromolecules (1–5 nm) (Field, 1993). A second approach, which applies well for macromolecules toward the top end of this range, considers the flux as being limited by the high osmotic pressure arising in the concentration-polarised layer close to the membrane surface, with no "gel" layer proposed (Vilker *et al.*, 1981; Wijmans *et al.*, 1984). Resistance models have also shown promise (Wijmans *et al.*, 1985). Other models, including the inertial migration models (Altena and Belfort, 1984), the shear-induced hydrodynamic convection (Davis and Birdsell, 1987) and diffusion (Romero and Davis, 1988, 1990) models, the erosion models (Fane *et al.*, 1982), the friction force models (Blake *et al.*, 1990), the particle

†Author to whom correspondence should be addressed.

adhesion models (Mackley and Sherman, 1992; Stamatakis and Chi Tien, 1993) and the pore-blocking models (Le and Howell, 1984), which in many cases claimed to predict filtration performance in the range 5 nm–10 μm, are only successful and applicable in the microfiltration range 500 nm–10 μm. The reason is the lack of attention to particle–particle interaction effects which are important in the colloidal size range of 5–500 nm.

Recent experimental investigations suggest that interparticle and especially electrostatic interactions play an important role in this particle range, in addition to hydrodynamic forces (applied in the above models). It has been found that increasing electrolyte concentration results in increased specific cake resistance in the filtration of suspensions of polystyrene or silica particles (Tadros and Mayes, 1980). This was interpreted in terms of a decrease in "effective particle size", that is, a reduction in Debye-length ($1/\kappa$). It has also been found that the permeability of layers of proteins formed at membrane surfaces during ultrafiltration depends on solution conditions (Reihanian *et al.*, 1983). Wakeman and Tarleton (1991) have found that varying the pH, and hence the zeta-potential, of anatase dispersions has a five-fold effect on filtration rate. Doshi and Trettin (1981) who investigated colloidal ultrafiltration in an unstirred batch cell favoured the hypothesis that in ultrafiltration of unflocculated or highly charged particles electrostatic interparticle repulsion has a sizeable effect upon the permeability of the subsequent filter cake that is formed. Altena and Belfort (1984) in their analysis of the lateral migration effect of spherical particles in porous flow channels mentioned that in addition to hydrodynamic forces, others such as electrokinetic forces, including London dispersion forces, electric double layer forces and hydrophobic interactions, may act on the particles. McDonogh *et al.* (1984, 1992) have reported the results of unstirred ultrafiltration of colloidal silica (and polystyrene) particles. Strong dependence of the specific resistance of the filter cake on the zeta-potential was found McDonogh *et al.* (1989) studied the charge effects in the cross-flow ultrafiltration of silica colloids. Increasing permeate flux (decreasing hydraulic resistance) with increasing zeta-potential for various cross-flow conditions was observed. This led them to the conclusion that the factors which control concentration polarisation on the membrane surface are charge dependent. These latter authors (McDonogh *et al.*, 1984, 1989, 1992) have also formulated a theoretical description of the ultrafiltration process that attempts to take electrostatic repulsive and London–van der Waals attractive interactions between particles into account. This was an important development, being the first attempt at quantification of the effect on ultrafiltration rate of two of the important types of interaction controlling the properties of concentrated colloids. However, their model development is highly simplified and contains an apparent misinterpretation of the Derjaguin–Landau–Verwey–Overbeek (DLVO) theory and the use of dimensionally incorrect and unverifiable equations. Further, the model development is for steady-state filtration only and does not take proper account of the dynamic nature of the ultrafiltration process. Other theoretical work has identified the importance of interparticle interactions, though only in outline form (Russel, 1987).

In aqueous colloidal systems, two types of interactions are always operative—electrostatic or double layer forces and London–van der Waals or dispersion forces. The summation of these forces forms the basis of the Derjaguin–Landau–Verwey–Overbeek (DLVO) theory of colloidal stability (Hunter, 1985). In practical applications of the DLVO theory, the electrostatic interactions are usually quantified in terms of zeta-potential (Hunter, 1981), the potential at the shear plane close to the particle surface as calculated from electrophoretic mobility measurements. The zeta-potential depends on pH, which affects the ionisation of surface groups, and ionic strength, with increasing ionic strength leading to decreased zeta-potential due to compaction of the diffuse double layer at the particle surface (decrease of Debye-length). More recently the importance of other interactions has been increasingly recognised (Israelachvili, 1991)—steric forces, hydration forces and hydrophobic forces. Gravitational and magnetic forces may in some circumstances also be significant. One of the most characteristic features of ultrafiltration of colloids is the production of a concentrated dispersion close to the membrane surface as the dispersed materials are separated from the liquid, which is transported through the membrane. Thus, it is very likely that the properties of this concentrated dispersion, which will be a result of the fundamental interactions between the colloidal particles, will have a significant influence on the separation efficiency of membrane ultrafiltration.

The preceding analysis of the ultrafiltration of colloidal dispersions leads to two conclusions. Firstly, that there is strong experimental evidence that particle–particle interactions have an important influence on the rate of ultrafiltration. Secondly, that there is a need for the development and application of a theory which rigorously takes such interactions into account. The present paper develops such a rigorous theory based on a Wigner–Seitz cell approach to account for multiparticle electrostatic interactions within the concentrated filter cake. The model also accounts for dispersion and hydration forces between the particles through an extended DLVO theory. The increase in configurational entropy due to the accumulation of particles above the membrane surface as well as electroviscous effects, i.e. an increased apparent fluid viscosity within the filter cake, have been considered. The model is a physics-based description of the filtration process with no adjustable parameters and accounts for the dynamic nature of membrane ultrafiltration. The model has been tested against experimental data for the ultrafiltration of well characterised silica colloids and excellent agreement is obtained between the theory and the experiment.

2. MODEL DEVELOPMENT: PARTICLE–PARTICLE INTERACTIONS

2.1. *The electrical double layer*

The simplest descriptions of surface–electrolyte interfaces treat the region in terms of an electrical double layer comprising a charged plane at the solid surface and a diffuse layer of counterions in the solution, the distribution of which is given by the Poisson–Boltzmann equation. This is known as the Gouy–Chapman model (Hunter, 1981), and treats the ions as being point charges at the surface. The finite size of real ions will, however, limit the inner boundary of the diffuse part of the double layer since the centre of an hydrated ion can approach the surface only to within its hydrated radius. Thus, a refinement is to divide the double layer into two parts separated by a plane, the Stern plane, located about a hydrated ion radius from the surface. This is termed the modified Gouy–Chapman model. Further refinement is also possible, for example, to distinguish between the Stern plane, also called the outer Helmholtz plane, and an inner Helmholtz plane. The ions in the inner Helmholtz plane are considered to be dehydrated, at least in the direction of the surface, and are said to be specifically adsorbed. This is known as the Gouy–Chapman–Stern–Graham or triple layer model. For the present macroscopic approach, the detailed structure of the inner regions of the double layer are not directly important. However, it is relevant that the position of the surface of shear at which the zeta-potential of particles may be calculated from electrophoretic mobility measurements is coincident with, or very close to, the outer Helmholtz plane (Hunter, 1981).

2.2. *Electrostatic interactions: double layer forces*

When two like particles approach each other close enough for their diffuse double layers to overlap they experience a repulsive electrostatic force which tends to oppose their further approach. In the classical DLVO theory this force has been considered in terms of a pairwise interaction approximation which made it strictly applicable only for dilute dispersions. However, in concentrated particle systems two characteristic phenomena may lead to errors. First, isolated pairs of particles are rare, and each particle's double layer overlaps that of several others, causing the interaction energy to depend on the configuration of many particles. Second, the entire volume of electrolyte interacts with the dispersed material. A basic assumption of the DLVO theory is that interacting particles are surrounded by a "bulk" region of fluid that acts as a source or sink for ions. In a concentrated dispersion this is no longer the case, and the screening of repulsion between charged particle surfaces is affected (Bell and Levine, 1957; Chen and Levine, 1972).

A cell model based on the Wigner and Seitz (1933) cell approach that attempts to account for these effects will be developed. This model has proved to be an excellent approximation for the grand canonical electrostatic potential energy of a concentrated particle system (Reiner and Radke, 1991). In this approach, the often complicated distribution of neighbours surrounding a particle is replaced by imagining that each particle in a concentrated stable dispersion is effectively isolated within a simplified (spherical, cylindrical, hexagonal, etc.) cell. In the present case of a spherical cell the outer cell boundary is normally chosen to result in the desired cell volume fraction of a polyhedron formed by the hexagonal close-packed particle geometry within the filter cake (see Section 3.1). An alternative choice for the location of this surface is one-half of the nearest neighbour separation, Fig. 1. The cell model approach will be solved by utilising an exact numerical solution to the full nonlinear Poisson–Boltzmann equation (PBE). This provides an applicability of the model for all surface potentials (zeta-potentials), ionic concentrations and interparticle distances.

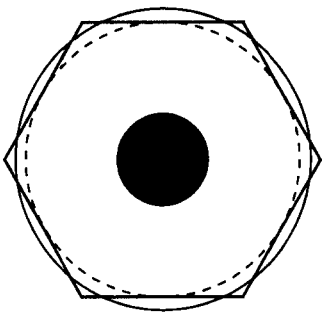

Fig. 1. Boundaries of the approximating spherical cell models. Dashed line shows nearest neighbour approach and solid line shows volume-equivalent approach to a polyhedron.

In general, the interaction of the double layers has been considered under conditions of constant surface potential, constant surface charge or charge regulation, the latter taking the chemistry of the surface explicitly into account (Chan and Mitchell, 1983). In most cases relevant to filtration, insufficient data is available for the application of charge regulation. For two identical surfaces, interaction at constant surface potential gives the lower bound for double layer repulsion, whereas interaction at constant surface charge gives the upper bound. The present paper will develop an analysis based on interaction at *constant zeta-potential.*

2.2.1. *Cell model approach.* The present cell model approach is based on the Wigner and Seitz (1933) cell model, which approximated the free electron energy of a crystal lattice by calculating the energy of a single crystal since it had the same symmetry as the lattice. The crystallographic symmetry planes were received by perpendicularly bisecting the lines to the nearest neighbours of an atom. This yielded that every atom was surrounded by a truncated octahedron which was approximated by a sphere of equal volume.

The colloidal filter cake is now divided into spherical cells, each containing a single particle, so that the

overall volume charge density within the cell is zero (electro-neutral). This kind of approach is a mean field approximation and accounts for the effect of averaging over all positions of neighbouring particles, i.e. considering multiparticle interactions, to yield the *configurational* electrostatic free energy per particle of the assemblage (Reiner and Radke, 1991). The cell volume (cell dimension) is given by the particle concentration in the filter cake.

The cell dimension (Fig. 1) can be arranged either to yield half of the nearest neighbour distance or to give the volume-equivalent of the polyhedron formed by the hexagonal close-packed particle packing geometry (see Section 3.1). Reiner and Radke (1991) showed that the volume-equivalent approach was superior over the half-distance case throughout their extensive comparison with a rigorous finite element solution of the configurational electrostatic free energy per particle in a concentrated colloidal system. Also, the volume-equivalent approach was in excellent quantitative agreement with their finite element solution. The volume-equivalent approach was therefore used in the present ultrafiltration model.

The resulting cell radius for the volume-equivalent approach, i.e. $V_{cell} = 4/3\pi r_{cell}^3 = V_{polyhedron}$, is given by the particle concentration or local voidage inside the filter cake via the hexagonal close-packed particle geometry:

$$r_{cell} = (2a + D)\left(\frac{3}{4\pi\sqrt{2}}\right)^{1/3}. \tag{1}$$

Hoskin and Levine (1956) showed that the repulsive force between two particles can generally be written as the derivative of the free energy of the double layers with respect to the interparticle centre–centre distance:

$$\frac{dG}{dR} = \int_S \left[\varepsilon_0\varepsilon_r\left((\mathbf{E}\cdot\mathbf{n})\mathbf{E} - \frac{1}{2}E^2\mathbf{n}\right) - (\Pi - \Pi_0)\mathbf{n}\right]dS \tag{2}$$

where S is any closed surface surrounding one of the particles only and $\mathbf{n}$ is the unit vector drawn outward to S.

Assuming identical spherical particles which are symmetrically orientated to one another eq. (2) can be modified to read

$$-\frac{dG}{dR} = \int_S \left(\frac{\varepsilon_0\varepsilon_r}{2}E^2 + (\Pi - \Pi_0)\right)dS \tag{3}$$

Applying the cell model approach to the derivative of the free energy of the double layer, eq. (3), results in

$$\begin{aligned} -\frac{dG}{dr_{cell}} &= \int_{S_{cell}} \left(\frac{\varepsilon_0\varepsilon_r}{2}E^2 + (\Pi - \Pi_0)\right)dS \\ &= \frac{\varepsilon_0\varepsilon_r}{2}\int_{S_{cell}} |\nabla\psi|^2\, dS \\ &\quad + 2n^0kT\int_{S_{cell}} \left(\cosh\frac{ze\psi}{kT} - 1\right)dS \end{aligned} \tag{4}$$

where S_{cell} is the outer cell surface.

Remembering that the cell is electrically neutral, i.e. that the charge density at the cell surface is zero and therefore from Gauss' theorem (Verwey and Overbeek, 1948)

$$\left.\frac{d\psi}{dr}\right|_{r=r_{cell}} = 0 \tag{5}$$

the configurational electrostatic free energy per particle is given by

$$\frac{dG}{dr_{cell}} = 2n^0kT\left(\cosh\frac{ze\psi|_{r=r_{cell}}}{kT} - 1\right)S_{cell}. \tag{6}$$

Bell and Levine (1957) and Feat and Levine (1974) have shown that multiparticle interactions in concentrated dispersions, i.e. the effect of averaging over all positions of neighbouring particles, are entirely described by the cell surface boundary condition [eq. (5)].

The configurational electrostatic free energy must be transformed into a repulsive force between two particles in the concentrated colloidal system. This is achieved by considering the particle packing geometry. In the present case, hexagonal close-packed is assumed, where a particle is surrounded by twelve nearest neighbours, as there is a considerable body of evidence that electrostatically stabilised dispersions exist in a structurally regular packing of minimum energy (Hiltner and Krieger, 1969; Kose *et al.*, 1973; Cohen *et al.*, 1993). Assuming that the forces are pairwise additive, the configurational electrostatic free energy is, therefore, equivalent to

$$-\frac{dG}{dr_{cell}} = 12f(D)\frac{1}{2} \tag{7}$$

where $f(D)$ is the repulsive force between two particles at an axial separation D and the factor $\frac{1}{2}$ is to avoid counting each particle–particle interaction twice (Guldbrand *et al.*, 1986; Reiner and Radke, 1991).

Substitution of eq. (7) into eq. (6) and rearranging yields for the force

$$f(D) = \frac{1}{3}S_{cell}\, n^0kT\left(\cosh\frac{ze\psi|_{r=r_{cell}}}{kT} - 1\right) \tag{8}$$

This repulsive force between two particles represents a "*configurational force*", which implicitly includes the electrostatic multi-body effects of a concentrated dispersion. This is in contrast to classical DLVO applications, where multiparticle effects are always treated on the basis of pairwise summation of interaction forces (or energies) of isolated pairs in bulk electrolyte solution.

2.2.2. *Solution to the non-linear Poisson–Boltzmann equation (PBE).* The electrostatic potential distribution inside the spherical cell will be described by the non-linear PBE for an open reservoir system limited to the case of a symmetric $z:z$ electrolyte. It has been demonstrated that in most practical situations the assumption of a symmetric electrolyte is not a serious restriction as the behaviour of colloidal systems is

largely governed by the counterions, so that it is also possible to treat an unsymmetrical electrolyte as symmetric (Verwey and Overbeek, 1948).

It is important to choose physically meaningful conditions at the particle surface when two charged surfaces approach one another. The most commonly studied condition is that of constant surface potential ψ_0. However, the problem which arises in choosing the right surface condition during double layer interactions depends mainly on the colloid material. The above assumption may be appropriate for metal sols in a solution where the metal is present in ionic form, and the surface charge is established by the adsorption of these ions onto the particle surfaces. On the other hand, if the particle charge is caused by structural crystal defects, as in some clay minerals, it might be more sensible to assume that the surface charge is constant during the approach of the particles (Hunter, 1985). In the case of biomaterials and oxide surfaces, the interaction may itself influence the degree of dissociation of surface groups so that neither ψ_0 nor σ_0 is constant. The condition known as charge regulation (Ninham and Parsegian, 1971) may then be more appropriate.

In the case of the metal oxides, the charge per unit area is determined by the number of dissociated groups at the particle surface. The surface potential is actually regulated by the dissociation mechanism as the particles are moved together, so that the boundary condition varies between the constant potential and constant charge extremes (Chan and Mitchell, 1983). However, consideration of such mechanisms requires the specification of additional parameters which depend on the dissociation model used. For instance, a single site-dissociation model, a two-site-dissociation model, or in particular, a site-dissociation site-binding model which accounts for binding of indifferent ions. The latter model requires knowledge of the dissociation and binding constants, the site density and the activity of the protons and indifferent ions adjacent to the particle surface (Miklavic and Ninham, 1990). To circumvent the introduction of other parameters, due to the charge regulation model for metal oxide particles, a simpler but still realistic approach has been developed.

When two charged surfaces approach one another under the condition of constant surface potential, the potential determining ions are driven off the surfaces until the double layers finally disappear on contact (Hunter, 1985). The absolute value of the potential profile $d\psi/dx$ at the surface, therefore, decreases. This can be interpreted as a decrease in the surface charge density, since $\sigma_0 = -\varepsilon_0\varepsilon_r(d\psi/dx)_{x=0}$. Hence, thermodynamic equilibrium must exist everywhere in the double layer, if this adjusting of the charge in the region between the approaching particles occurs rapidly, so that at each moment the charge distribution varies with the interparticle distance. On the other hand, if the particles approach each other under the constant surface charge condition, no thermodynamic equilibrium is established, as no ionic transport from one phase to another occurs when the distance between the surfaces is varied. Therefore, only the electric part of the free energy changes, which is obtained by an increasing surface potential. It is known that an increase in electrolyte concentration diminishes the thickness of the double layer and also causes an increased adsorption of hydroxyl ions onto the surface to maintain overall electric neutrality, which raises the surface potential, so that the overall zeta-potential, i.e. the potential at the plane of shear (or outer Helmholtz plane) a distance d from the particle surface, remains relatively unchanged (Iler, 1979).

Thus, under *constant zeta-potential* conditions the potential determining ions are driven off the surface when a dispersion gets more concentrated (or because of a build-up of a filter cake) and therefore contribute to an increase in the electrolyte concentration (Benzing and Russel, 1981; Beunen and White, 1981), which results in thinner double layers and further in higher surface potentials. The approach fulfils the general charge regulation principle and the assumption of constant zeta-potential seems to be adequate. Therefore, the modified Gouy–Chapman model of the double layer has been applied under a constant zeta-potential condition.

Calculating the configurational electrostatic repulsive force [eq. (8)] in terms of the spherical cell model requires that the non-linear PBE must be solved for spherical geometry and that the electrostatic potential in the fluid, i.e. at the cell boundary, must be found as a function of the cell dimension. The PBE in spherical coordinates reads as follows:

$$\frac{d^2\psi}{dr^2} + \frac{2}{r}\frac{d\psi}{dr} = \frac{2n^0 ze}{\varepsilon_0\varepsilon_r}\sinh\left(\frac{ze\psi}{kT}\right). \tag{9}$$

The PBE may be normalised using the following substitutions:

$$\Psi = \frac{ez\psi}{kT} \tag{10}$$

$$R = \kappa r \tag{11}$$

$$\kappa = \left(\frac{e^2\sum z^2 n^0}{\varepsilon_0\varepsilon_r kT}\right)^{1/2} = \left(\frac{2e^2z^2N_A I}{\varepsilon_0\varepsilon_r kT}\right)^{1/2}. \tag{12}$$

The normalised PBE becomes

$$\frac{d^2\Psi}{dR^2} + \frac{2}{R}\frac{d\Psi}{dR} = \sinh\Psi \tag{13}$$

which must be solved between the limits of $\alpha \leqslant R \leqslant \beta$, where $\alpha = \kappa(a + d)$ and $\beta = \kappa r_{cell}$ with $r_{cell} \geqslant a + d$.

The boundary condition at $R = \alpha$ is determined by the constant zeta-potential

$$\Psi|_{R=\alpha} = \xi = \frac{ze\zeta}{kT}. \tag{14}$$

Since the total charge on the particle surface and in the surrounding fluid is zero, from Gauss' theorem, the electric field normal to the sphere surface must also be zero [see eq. (5)]. At $R = \beta$, the second bound-

ary condition is

$$\left.\frac{d\Psi}{dR}\right|_{R=\beta} = 0. \tag{15}$$

Equations (9)–(15) specify the problem. However, the hyperbolic sine term in the PBE makes the second-order differential equation exponentially non-linear. The solution will be very steep near $R = \alpha$, which suggests a "stiff" equation (Acton, 1970). To avoid this problem, an extension of an approach performed by Strauss *et al.* (1987) will be adopted, i.e. a transformation of Ψ.

Strauss *et al.* (1987) suggested that using the solution to the PBE for a single flat plate in an infinite electrolyte solution as a model equation, the potential distribution Ψ may be expressed as

$$\Psi = 4 \operatorname{arctanh} [M(R)] \tag{16}$$

where $M(R)$ is some function of distance away from the particle surface. Equation (16) can be substituted into the normalised PBE to yield the equation in terms of function M.

Therefore, eq. (16) is differentiated with respect to R

$$\frac{d\Psi}{dR} = \frac{4}{1 - M^2}\frac{dM}{dR}. \tag{17}$$

The second derivative of eq. (16) gives

$$\frac{d^2\Psi}{dR^2} = \frac{4}{1 - M^2}\frac{d^2M}{dR^2} + \frac{8M}{(1 - M^2)^2}\left(\frac{dM}{dR}\right)^2. \tag{18}$$

The right-hand side of eq. (13) can be expressed as follows:

$$\sinh \Psi = 4 \sinh\left(\frac{\Psi}{4}\right)\cosh\left(\frac{\Psi}{4}\right)\left[1 + 2\sinh^2\left(\frac{\Psi}{4}\right)\right]. \tag{19}$$

Since $M = \tanh(\Psi/4)$ from eq. (16) and

$$\sinh\frac{\Psi}{4} = \frac{\tanh\frac{\Psi}{4}}{\sqrt{1 - \tanh^2\frac{\Psi}{4}}}, \quad \cosh\frac{\Psi}{4} = \frac{1}{\sqrt{1 - \tanh^2\frac{\Psi}{4}}}$$

a substitution in eq. (19) results in

$$\sinh \Psi = \frac{4M}{1 - M^2} + \frac{8M^3}{(1 - M^2)^2}. \tag{20}$$

Substituting eqs (17), (18) and (20) into the normalised PBE [eq. (13)] and rearranging yields

$$\frac{d^2M}{dR^2} + \frac{2}{R}\frac{dM}{dR} + \frac{2M}{1 - M^2}\left(\frac{dM}{dR}\right)^2 = \frac{M(1 + M^2)}{1 - M^2}. \tag{21}$$

Although eq. (21) seems more complex than eq. (13), it has the advantage that the hyperbolic sine term is missing. However, eq. (21) is still non-linear, but since it contains only polynomial terms and not exponential terms, it is not as stiff as eq. (13). The range of M is bounded between -1 and $+1$, while Ψ ranges from $-\infty$ to $+\infty$. As the PBE is stiff, errors in the potential can grow beyond the numerical limits of a computer if Ψ is used (Strauss *et al.*, 1987). If M is used propagation of errors can only increase M to a value of one.

The two boundary conditions, eqs (14) and (15), may be transformed in terms of the function M, via eqs (16) and (17), respectively, to read

$$M|_{R=\alpha} = \tanh\frac{\xi}{4} = M_\xi \tag{22}$$

$$\left.\frac{dM}{dR}\right|_{R=\beta} = 0. \tag{23}$$

To solve the above boundary-value problem a starting value for the desired potential (or M) at β is given by the solution to the linearised PBE, i.e. the Debye–Hückel solution, which is valid at low potentials and can be solved analytically. Its solution will not generally be accurate, but it is adequate as a first guess. The linearised PBE is given by

$$\frac{d^2\Psi}{dR^2} + \frac{2}{R}\frac{d\Psi}{dR} = \Psi \tag{24}$$

The solution to this equation is

$$\Psi = \frac{A}{R}e^{(R-\alpha)} + \frac{B}{R}e^{-(R-\alpha)} \tag{25}$$

where A and B are constants determined by the boundary conditions. If the solution, eq. (25), is applied to the two boundary conditions, eqs (14) and (15), the constants are

$$A = \frac{\xi\alpha e^{-2(\beta-\alpha)}}{\frac{\beta - 1}{\beta + 1} + e^{-2(\beta-\alpha)}} \tag{26}$$

$$B = \xi\alpha - A \tag{27}$$

which yields at $R = \beta$

$$\Psi(\beta) = \frac{A}{\beta}e^{\beta-\alpha} + \frac{\xi\alpha - A}{\beta}e^{-(\beta-\alpha)}. \tag{28}$$

Equation (28) provides an initial guess for the potential at the cell boundary, which may be transformed into $M(\beta)$ by eq. (16) to yield

$$M(\beta) = \tanh\frac{\Psi(\beta)}{4}. \tag{29}$$

$M(\beta)$ is used as a starting point to estimate the value of M at the next segment $(i - 1)$ in the interval $(\beta - \alpha)$. The values of M at each segment, i, of the potential distribution curve are obtained by a third-order Taylor's expansion for M and a second-order Taylor's expansion for its derivative dM/dR:

$$M_{i-1} = M_i - M_i'\Delta_i + \frac{M_i''}{2}\Delta_i^2 - \frac{M_i'''}{6}\Delta_i^3 \tag{30}$$

$$M_{i-1}' = M_i' - M_i''\Delta_i + \frac{M_i'''}{2}\Delta_i^2. \tag{31}$$

Here, the primes denote derivatives with respect to R and Δ_i is the variable spacing between discrete

points determined by a per step truncation error calculation explained later.

The first derivative of function M with respect to R is given by the boundary condition equation (23). The second derivative follows from rearranging eq. (21):

$$\frac{d^2M}{dR^2} = \frac{M(1+M^2)}{1-M^2} - \frac{2}{R}\frac{dM}{dR} - \frac{2M}{1-M^2}\left(\frac{dM}{dR}\right)^2. \tag{32}$$

The third derivative is found by taking the derivative of eq. (32):

$$\begin{aligned}\frac{d^3M}{dR^3} = &\left[\frac{2M^2+2M^4}{(1-M^2)^2} + \frac{1+3M^2}{1-M^2}\right]\frac{dM}{dR} \\ &- \left[\frac{2}{R}\frac{d^2M}{dR^2} - \frac{2}{R^2}\frac{dM}{dR}\right] \\ &- \left[\left(\frac{4M^2}{(1-M^2)^2} + \frac{2}{1-M^2}\right)\left(\frac{dM}{dR}\right)^3 \right. \\ &\left. + \frac{4M}{1-M^2}\frac{dM}{dR}\frac{d^2M}{dR^2}\right]\end{aligned} \tag{33}$$

which differs from that given by Strauss *et al.* (1987) which is given incorrectly. The truncation error in M_i may be estimated for each segment to

$$T_i \cong \frac{M_i''''}{24}\Delta_i^4 \tag{34}$$

where M_i'''' is the fourth derivative given by

$$\begin{aligned}\frac{d^4M}{dR^4} = &\left[\frac{8M^3+8M^5}{(1-M^2)^3} + \frac{6M+14M^3}{(1-M^2)^2} \right. \\ &\left. + \frac{6M}{1-M^2}\right]\left(\frac{dM}{dR}\right)^2 + \left[\frac{2M^2+2M^4}{(1-M^2)^2} \right. \\ &\left. + \frac{1+3M^2}{1-M^2}\right]\frac{d^2M}{dR^2} - \left[\left(\frac{2}{R}\frac{d^3M}{dR^3} - \frac{2}{R^2}\frac{d^2M}{dR^2}\right)\right. \\ &\left. - \left(\frac{2}{R^2}\frac{d^2M}{dR^2} - \frac{4}{R^3}\frac{dM}{dR}\right)\right] \\ &- \left[\frac{16M^3}{(1-M^2)^3} + \frac{12M}{(1-M^2)^2}\right]\left(\frac{dM}{dR}\right)^4 \\ &- \left[\frac{12M^2}{(1-M^2)^2} + \frac{6}{1-M^2}\right]\left(\frac{dM}{dR}\right)^2\frac{d^2M}{dR^2} \\ &- \left[\frac{8M^2}{(1-M^2)^2}\left(\frac{dM}{dR}\right)^2 + \frac{4M}{1-M^2}\frac{d^2M}{dR^2}\right] \\ &\times \frac{d^2M}{dR^2} - \left[\frac{4M}{1-M^2}\frac{dM}{dR}\right]\frac{d^3M}{dR^3}.\end{aligned} \tag{35}$$

A relative truncation error ΔT_i is defined as

$$\Delta T_i = \frac{\frac{M_i''''}{24}\Delta_i^4}{\frac{M_i'''}{6}\Delta_i^3} = \frac{1}{4}\frac{M_i''''}{M_i'''}\Delta_i \tag{36}$$

and used to predict the next interval step size, while the required relative truncation error ΔT_{req} is kept constant, i.e.

$$\Delta_{i-1} = \Delta_i \frac{\Delta T_{req}}{\Delta T_i}. \tag{37}$$

The relative truncation error in the $(i-1)$ step is again checked against the required relative truncation error and, if necessary, the step size corrected by an iterative predictor–corrector schema to yield the required relative truncation error. The variable step size procedure yields a minimum amount of steps to be calculated in the interval $(\beta - \alpha)$ and allows a control on the per step accuracy as well.

The extrapolation of M_i and M_i' is carried out until α is reached. At this point the value of the extrapolated boundary condition $M_{i=n}$ is compared with the correct value M_ξ [eq. (22)]. A false-position interpolation is applied to obtain a better guess for $M(\beta)$ (or $M_{i=0}$). The relationship used for the false-position interpolation is

$$M_0^{k+1} = \frac{M_0^k(M_n^{k-1} - M_\xi) - M_0^{k-1}(M_n^k - M_\xi)}{M_n^{k-1} - M_n^k} \tag{38}$$

where M_0^k is the kth guess for $M(\beta)$. The iterative process is continued until M_n^k is within 0.01% of the correct boundary value M_ξ.

For the first false-position iteration a M_0^{k-1} guess is needed other than the M_0^k guess obtained from the Debye–Hückel approximation. The solution $M_0^{k-1} = 0$, i.e. $\Psi_{R=\beta} = 0$, is used, which implies that the extrapolated value M_n^{k-1} is also zero.

The above method calculates the potential distribution at one value of the cell dimension or local filter cake voidage. Substituting the value of the potential at the outer cell boundary into eq. (8) provides the configurational electrostatic force between two particles for a given local filter cake voidage (or interparticle spacing).

2.3. *London–van der Waals interactions: dispersion forces*

In the first quantum-mechanical treatment of van der Waals forces, the weak attractive forces acting between all molecules, it was assumed that these forces were additive, so that in large collections of molecules the total interaction energy was not different from the sum of the pairwise interaction energies (London, 1930). This allowed the introduction of a simple procedure for the calculation of the attractive London–van der Waals forces between macrobodies by the pairwise summation of intermolecular forces (Hamaker, 1937). This led to expressions for calculation of total attractive interaction energy, which for the case of two spheres is given by

$$\begin{aligned}V_A(D) = -\frac{A_H}{6}&\left[\frac{2a^2}{D^2+4aD} + \frac{2a^2}{(D+2a)^2} \right. \\ &\left. + \ln\left(1 - \frac{4a^2}{(D+2a)^2}\right)\right].\end{aligned} \tag{39}$$

This represents an approximation to reality as the internal states of molecules will be affected by the

presence of all other molecules. The approximation of additivity is completely avoided by modern dispersion force theory (Lifshitz, 1956; Dzyaloshinskii, 1961) as the atomic structure is ignored and the forces between large bodies, now treated as continuous media, are derived in terms of such bulk properties as their dielectric constants and refractive indices. However, the full theory involves statistical mechanical and quantum field theory of a complexity outside the scope of the present assessment of filtration. Indeed, two further factors complicate the calculation of attractive interactions. Firstly, the phenomenon of retardation, which arises due to the finite time for the transmission of electromagnetic radiation. This leads to the Hamaker constant never being truly constant but decreasing progressively as D increases. It can, for example, fall from its full non-retarded value at small D to less than half this value at $D = 10$ nm (Israelachvili, 1991). Secondly, electromagnetic interactions are screened in electrolyte solutions (Mahanty and Ninham, 1976).

For the present work, there is a need to adopt a procedure for calculation of dispersion forces which accurately represents the results of modern theory yet has only moderate computational needs (Bowen and Jenner, 1995b). The approach to be adopted is to use an effective Lifshitz–Hamaker constant for flat plates with the Hamaker geometrical factor for spheres, as first suggested in the most comprehensive treatment of dispersion forces (Mahanty and Ninham, 1976). Comparison of such an approach (Pailthorpe and Russel, 1982) for polystyrene spheres in water, using an exact screened, retarded, planar Lifshitz–Hamaker constant, showed excellent agreement with the exact Lifshitz solution (Langbein, 1970). With geometrical effects accounted for in this way, the remaining problem is to find a computationally efficient means of calculating the Lifshitz–Hamaker constant.

A simplified approach to such calculation that sacrifices some accuracy but reduces both the numerical effort and the number of parameters characterising the individual materials has been presented (Horn and Israelachvili, 1981; Prieve and Russel, 1988; Russel *et al.*, 1989). The development is based on observations that relaxations in the ultraviolet dominate the portion of the dielectric spectra most important for dispersion interactions (Hough and White, 1980; Israelachvili, 1991). Based on this approach, the Lifshitz–Hamaker constant can be calculated from

$$A_{131}(\kappa, D) = A_{\xi_0}(1 + 2\kappa D)e^{-2\kappa D} + A_{\xi_{\gg 1}}F(H) \quad (40)$$

with

$$A_{\xi_0} = \frac{3}{4}kT\left[\frac{\varepsilon_{r_1}(0) - \varepsilon_{r_3}(0)}{\varepsilon_{r_1}(0) + \varepsilon_{r_3}(0)}\right]^2$$

$$A_{\xi_{\gg 1}} = \frac{3h\sqrt{\omega_1\omega_3}}{64\bar{n}_0^{7/4}} \times \frac{X^2\bar{n}_0 + 2X\,\Delta n_0\sqrt{\bar{n}_0} + \Delta n_0^2(3 + 2Y)}{[(Y - \sqrt{Y^2 - 1})^{1/2} + (Y + \sqrt{Y^2 - 1})^{1/2}]^3}$$

$$\bar{n}_0 = \frac{n_{0_1} + n_{0_3}}{2}$$

$$\Delta n_0 = n_{0_1} - n_{0_3}$$

$$X = \frac{\omega_1}{\omega_3}(n_{0_1} - 1) - \frac{\omega_3}{\omega_1}(n_{0_3} - 1)$$

$$Y = \frac{1}{4\sqrt{\bar{n}_0}}\left[\frac{\omega_1}{\omega_3}(n_{0_1} + 1) + \frac{\omega_3}{\omega_1}(n_{0_3} + 1)\right]$$

$$F(H) = \left[1 + \left(\frac{\pi H}{4\sqrt{2}}\right)^{3/2}\right]^{-2/3}$$

$$H = n_{0_3}(n_{0_1}^2 - n_{0_3}^2)^{1/2}\frac{D\sqrt{\omega_1\omega_3}}{c}.$$

The first term A_{ξ_0} in eq. (40) gives the zero-frequency energy of the van der Waals interaction and includes the Keesom and Debye dipolar contributions. This term remains non-retarded at all separations but is subject to screening in electrolyte solutions (Mahanty and Ninham, 1976; Israelachvili, 1991), as shown in the equation. The second term $A_{\xi_{\gg 1}}$ gives the dispersion energy and includes the London energy contribution. It is subject to retardation. This term is given in a form that allows for the medium across which interaction is taking place to have a different adsorption frequency to that of the interacting bodies.

The characteristic frequencies in eq. (40) can be obtained by experimentally measuring the refractive index as a function of wavelength and analysing the data using a Cauchy plot (Hough and White, 1980). For the experimental system used in the present work, such Cauchy plot analysis was based on extensive refractive index data for fused silica (Malitson, 1965). For the case of non-retarded, non-screened Lifshitz–Hamaker constants it is found that the present analysis gives a value of $A_{131} = 0.795 \times 10^{-20}$ J for silica which compares well with the exact value of $A_{131} = 0.849 \times 10^{-20}$ J (Hough and White, 1980). The importance of including an electrolyte screening term can be seen from the following calculated data:

$$A_{\xi_0}(\kappa D = 0) = 0.251 \times 10^{-20}\text{ J}$$
$$A_{\xi_0}(\kappa D = 1) = 0.102 \times 10^{-20}\text{ J}$$
$$A_{\xi_0}(\kappa D = 2) = 0.023 \times 10^{-20}\text{ J}$$
$$A_{\xi_0}(\kappa D = 3) = 0.004 \times 10^{-20}\text{ J}.$$

The dispersion force between two spherical particles is thus given by the derivative of the attractive interaction energy with respect to distance

$$F_A = -\frac{1}{6}\left\{\left[A_{\xi_0}4\kappa^2 De^{-2\kappa D} + A_{\xi_{\gg 1}}\left(1 + \left(\frac{\pi H}{4\sqrt{2}}\right)^{3/2}\right)^{-5/3} \times \left(\frac{\pi}{4\sqrt{2}}n_{0_3}\sqrt{n_{0_1}^2 + n_{0_3}^2}\frac{\omega_1}{c}\right)^{3/2}\sqrt{D}\right]\right.$$

$$\times\left[\frac{2a^2}{D^2+4aD}+\frac{2a^2}{(D+2a)^2}\right.$$
$$\left.+\ln\left(1-\frac{4a^2}{(D+2a)^2}\right)\right]$$
$$+[A_{\xi_0}(2\kappa D+1)e^{-2\kappa D}+A_{\xi_{\geq 1}}F(H)]$$
$$\times\left[2a^2\left(\frac{2D+4a}{(D^2+4aD)^2}+\frac{2}{(D+2a)^3}\right.\right.$$
$$\left.\left.-\frac{4}{(D+2a)^3-4a^2D-8a^3}\right)\right]\Bigg\}. \quad (41)$$

2.4. *Non-DLVO forces*

The stability of some colloids is known to be irregular in the sense that they do not follow the predictions of the standard DLVO theory (Israelachvili, 1991). The test system to be used in the present work, silica, is such a colloid as it exhibits an additional short-range repulsive force (Ducker *et al.*, 1992; Grabbe and Horn, 1993). The reasons for this are not clear, and there is no fundamental theory to describe the interaction. The force has been attributed to hydration of the surface and has been shown to be affected neither by surface treatments nor by electrolyte concentration up to 0.1 M. Experimental work using thin sheets of silica in a surface force apparatus (Grabbe and Horn, 1993) has shown that the force may be expressed as the sum of two exponential terms, which for spheres may be written,

$$F_{hyd}(D)=\pi a[F_1\exp(-D/D_1)+F_2\exp(-D/D_2)] \quad (42)$$

with $F_1=0.14\,\mathrm{J\,m^{-2}}$, $D_1=0.057\times10^{-9}\,\mathrm{m}$, $F_2=5.4\times10^{-3}\,\mathrm{J\,m^{-2}}$ and $D_2=0.48\times10^{-9}\,\mathrm{m}$.

2.5. *DLVO theory*

The central concept of the DLVO theory (Derjaguin and Landau, 1941; Verwey and Overbeek, 1948) is that the total interaction energy of two surfaces or particles is given by the summation of the attractive and repulsive contributions. This may be written in extended form as

$$V_T=V_R+V_A+V_S \quad (43)$$

where the total interaction energy (V_T) is expressed in terms of the repulsive electrostatic interaction energy (V_R) and the attractive London–van der Waals interaction energy (V_A), as in the original theory, with the additional term (V_S) representing additional short-range forces, which could be repulsive hydration forces or attractive hydrophobic forces depending on the system under study.

2.6. *Configurational entropy*

When molecules or colloidal particles are forced close together within a dispersion their entropic pressure (or osmotic pressure) will increase due to an ordering of the particles which decreases their degree of freedom to move in free fluid space.

Carnahan and Starling (1969) derived the equation of state for rigid spheres within the fluid (disordered state) expressed in terms of an entropic pressure

$$p_{ent}=\left(\frac{3\phi}{4\pi a^3}\right)kT\frac{(1+\phi+\phi^2-\phi^3)}{(1-\phi)^3} \quad (44)$$

where ϕ is the particle volume fraction. Equation (44) is the most accurate closed-form equation and agrees with both the first seven virial coefficients and molecular dynamics results (better than 0.5%) (Hall, 1972; Russel *et al.*, 1989).

Molecular dynamics and Monte Carlo simulations and statistical mechanical theories for hard spheres predict a transition from a disordered phase for ($\phi<0.5$) to a face-centred-cubic (or h.c.p.) ordered phase for ($0.55>\phi>0.74$) (see Russel *et al.*, 1989). Since eq. (44) strictly applies only for the disordered state ($\phi<0.5$), Hall (1972) derived a closed-form expression for the ordered state ($\phi>0.55$),

$$p_{ent}=\left(\frac{3\phi}{4\pi a^3}\right)kT\begin{pmatrix}2.558+0.125\beta+0.176\beta^2-1.053\beta^3\\+2.819\beta^4-2.922\beta^5+1.118\beta^6+(12-3\beta)/\beta\end{pmatrix} \quad (45)$$

with $\beta=4[1-6\phi/(\pi\sqrt{2})]$, which gives accurate results (better than 0.02%) compared with molecular dynamics data (data available up to $\phi=0.7331$).

Figure 2 displays the configurational entropic pressure over the full range of particle concentration, indicating the disordered [eq. (44)] and ordered [eq. (45)] phases, as well as a continuous approximation from Hall (1972) which covers both regions:

$$p_{ent}=\left(\frac{3\phi}{4\pi a^3}\right)kT\,\frac{(1+\phi+\phi^2-0.67825\phi^3-\phi^4-0.5\phi^5-X\phi^6)}{(1-3\phi+3\phi^2-1.04305\phi^3)} \quad (46)$$

where

$$X=6.028\exp[Y(7.9-3.9Y)]$$
$$Y=\frac{\pi\sqrt{2}}{6}-\phi.$$

If a filter cake is considered, where at least random loose packing ($\phi=0.555$) but more likely random close packing ($\phi=0.645$) (Onoda and Liniger, 1990) or hexagonal close packed and face-centred cubic of uniform spherical particles is assumed, the Hall approximation seems to be a reasonable representation of the configurational entropic pressure. However, it can be assumed due to experimental evidence (Hiltner and Krieger, 1969; Hachisu *et al.*, 1973; Cohen *et al.*, 1993; Philipse and Pathmamanoharan, 1993) that the

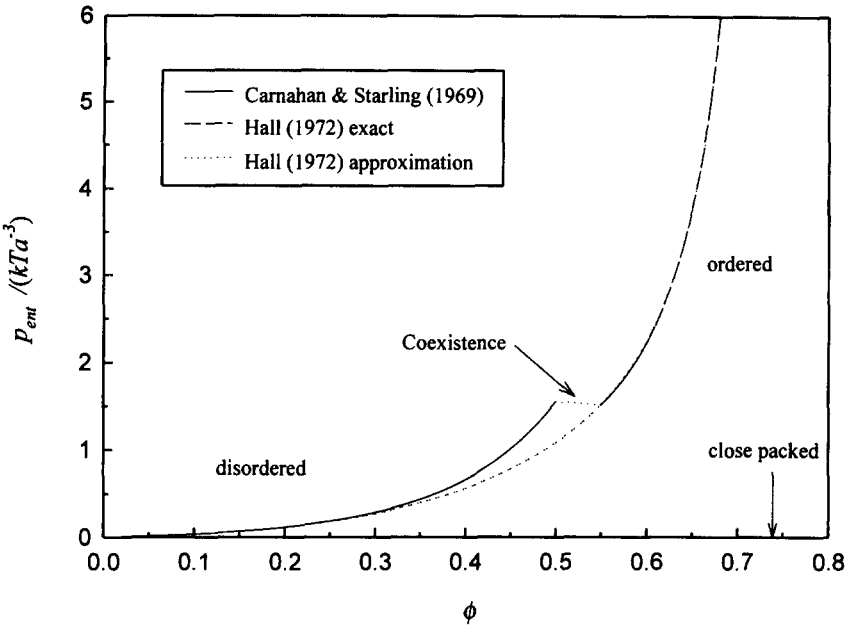

Fig. 2. Configurational entropic pressure for hard sphere dispersions including the disordered and ordered curves and the coexistence region for $0.5 < \phi < 0.55$. The dashed line represents Hall's (1972) continuous approximation.

particles are in an ordered state within the filter cake even for high electrolyte concentrations.

2.7. *Electroviscous effects*

The consequences of applying pressure and potential gradients across capillaries (or porous media) filled with electrolyte are well known (viz., electro-osmosis, streaming potential and electroviscous effects) (Hunter, 1981). When, for example, an electrolyte flows through electrically charged capillaries (or porous media) under a pressure gradient, the charges in the mobile part of the double layer near the wall are carried towards one end. This constitutes a streaming current (or convective current), I_s, and the accumulation of charge sets up an electric field. The field causes a current flow in the opposite direction through the bulk of the liquid and when the latter conduction current, I_c, is equal to the streaming current, a steady state is achieved. The resulting electrostatic potential difference between the ends of the capillary is the *streaming potential*. This potential will produce a backflow of liquid by the *electro-osmotic effect*, i.e. the counterions in the double layer adjacent to the capillary wall will move under the influence of the induced electric field and they will draw the liquid along with them. The net effect is a diminished flow in the forward direction. The liquid appears to exhibit an enhanced viscosity, if its flow rate is compared with the flow in the absence of double layer effects (e.g. at high salt concentration or at the point of zero charge). This increase in apparent viscosity of the fluid refers to the so called *electroviscous effect*.

The basic relationships involved were formulated long ago, mainly by Smoluchowski (1918). However, these relationships suffered from a severe restriction due to the assumption that the electrokinetic radius κr_c had to be very large, i.e. that the double layer thickness $(1/\kappa)$ is small compared to the capillary radius (r_c). Rice and Whitehead (1965), in their publication on electrokinetic flow in a narrow cylindrical capillary, have calculated analytically the correction factors that must be applied to Smoluchowski's results when dealing with narrow capillaries having arbitrary values of κr_c $(0 < \kappa r_c < \infty)$. However, Rice and Whitehead's theory itself is subject to the severe restriction that the zeta-potential be sufficiently low to permit the Debye–Hückel approximation, effectively limiting the application of their predictions to $\zeta \leqslant 25\,\text{mV}$ for a monovalent electrolyte. Levine *et al.* (1975) have extended the theory of Rice and Whitehead to higher zeta-potentials by developing analytical approximations to the solution of the non-linear PBE within the capillary. However, Levine's analysis of the electroviscous effect is confined to a symmetric monovalent electrolyte having equal ionic mobilities. Bowen and Jenner (1995c) extended the approach of Levine *et al.* (1975) for the case of a symmetric electrolyte with arbitrary ionic mobilities. The full non-linear PBE has been solved numerically in cylindrical coordinates to be applicable for all zeta-potentials. Approximated theoretical predictions of the apparent fluid viscosity of Levine *et al.* (1975) have been found to be in very good agreement with Bowen and Jenner's (1995b) numerical results. The final equation for the apparent viscosity was

$$\frac{\mu_a}{\mu} = \left[1 - \frac{8\varepsilon_0\varepsilon_r\xi^2}{\mu}(1-G)^2\left(\frac{2\varepsilon_0\varepsilon_r}{\mu}\int_0^{R_c} R(\mathrm{d}\Psi/\mathrm{d}R)^2\,\mathrm{d}R \times\left(\frac{ze}{kT}\right)\int_0^{R_c} R(m_+e^{-\Psi(R)} + m_-e^{\Psi(R)})\,\mathrm{d}R\right)^{-1}\right]^{-1} \quad (47)$$

with

$$G = \frac{2}{R_c^2\xi}\int_0^{R_c} R\Psi(R)\,\mathrm{d}R, \quad R = \kappa r, \quad R_c = \kappa r_c.$$

Bowen and Jenner (1995b) applied the model to porous media (e.g. filter cakes) by introducing an equivalent hydraulic radius of a cylindrical capillary for the capillary channels within the filter cake (Kozeny, 1927). For spherical particles of equal size this gives

$$r_{c,\mathrm{hyd}} = \frac{\varepsilon}{(1-\varepsilon)}\frac{(a+d)}{3} \quad (48)$$

which is a function of the cake voidage (or interparticle spacing).

3. MODEL DEVELOPMENT: FILTRATION THEORY

During "dead-end" ultrafiltration the filtered particles build-up on the membrane surface forming a filter cake. The rate of filtration then depends on the hydraulic resistance of this cake. Such resistance depends on the interparticle spacing, which depends on the interactions between the particles. The following sections describe a dynamic model for the filtration of colloidal particles which uses an extended DLVO theory to describe such interactions. Configurational entropy and electroviscous effects are also taken into account.

3.1. *Dynamic model development*

The starting point for the present ultrafiltration model are the fundamental equations describing the repulsive configurational electrostatic interactions between particles [eq. (8)], the attractive London–van der Waals interactions [eq. (41)] and the hydration interactions [eq. (42)] as combined by the DLVO theory [eq. (43)]. The increase in configurational entropy due to the accumulation of particles above the membrane surface as well as electroviscous effects, i.e. an increased apparent fluid viscosity within the filter cake, are also considered.

There is a considerable body of evidence that electrostatically stabilised dispersions exist in a structurally regular packing form of minimum energy (Hiltner and Krieger, 1969; Kose *et al.*, 1973; Cohen *et al.*, 1993). For concentrated and highly concentrated dispersions the assumption that colloids are ordered in a hexagonal close-packed (h.c.p.) or face-centred cubic (f.c.c.) [also called cubic close-packed (c.c.p.)] geometry is supported. Both give the highest possible limiting packing density ($\phi = 0.7404$). The first task in the development of the present model is to apply the equations for interaction of pairs of particles in a way

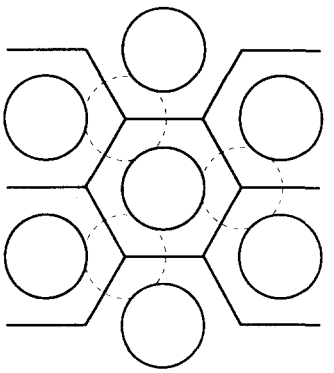

Fig. 3. Schematic representation of a hexagonal close-packed array, showing the three adjacent neighbours in the contiguous layer (broken circles) and the hexagonal effective area per particle.

appropriate to the multiple interactions which will occur in a structured filter cake. A method which allows the calculation of the forces per unit area between particles of hexagonal close-packed concentrated dispersions from the total interaction energies (or forces) for pairs of particles will be used (Evans and Napper, 1978). In this approach the forces per unit area perpendicular to the filter cake, which may be termed the "disjoining pressure" (p_D) (Derjaguin *et al.*, 1964), on one side of a hypothetical plane inserted between two contiguous layers in the hexagonal close-packed array are calculated, Fig. 3. The effective area, A_h, occupied per particle at the hypothetical plane is that of a regular hexagon constructed about an inscribed circle of radius $(a + D/2)$:

$$A_h = 2\sqrt{3}(a + D/2)^2. \quad (49)$$

The force on each particle at the hypothetical plane is transmitted equally from three other particles in the contiguous layer of the array, the centres of the four particles forming the apices of a regular tetrahedron. The disjoining pressure is then given by

$$p_D = \frac{\sqrt{6}}{A_h}F_T = \frac{\sqrt{6}}{A_h}[f(D) + F_A(D) + F_{\mathrm{hyd}}(D)] \quad (50)$$

where $f(D)$ is the configurational electrostatic force between two particles [eq. (8)], $F_A(D)$ is the Lifshitz dispersion force [eq. (41)] and $F_{\mathrm{hyd}}(D)$ is the hydration force [eq. (42)]. For the present model developement only nearest neighbours are considered, due to the computational time and effort necessary in solving the non-linear PBE. On the other hand, since the configurational electrostatic free energy is transformed into nearest neighbour pair interactions, it is consistent to treat also only nearest neighbours in the Evans and Napper (1978) approach. The configurational entropic pressure term, eq. (46), will be added to the total disjoining pressure and finally gives

$$p_D = \frac{\sqrt{6}}{A_h}[f(D) + F_A(D) + F_{\mathrm{hyd}}(D)] + p_{\mathrm{ent}}. \quad (51)$$

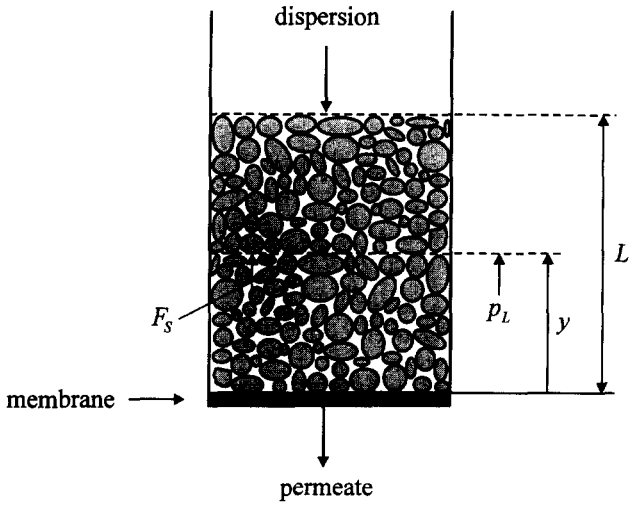

Fig. 4. Schematic diagram of forces and pressures acting in a filter cake.

To calculate the voidage of the filter cake, the disjoining pressure of eq. (51) must be related to the applied ultrafiltration pressure. Pressure within filter cakes may be analysed in terms of the local compressive drag and hydraulic forces on particles (Tiller *et al.*, 1980), Fig. 4. The compressive drag force is cumulative throughout the cake, increasing from zero at the cake-dispersion interface to a maximum value at the membrane surface. A force balance may then be written

$$F_S + p_L A = \Delta p_C A. \tag{52}$$

Assuming uniform pressure in any plane perpendicular to the direction of flow, and defining a compressive drag pressure, $p_S = F_S A$, it is possible to write

$$p_S + p_L = \Delta p_C \tag{53}$$

where p_S, the local compressive drag pressure, is the "effective pressure" of soil mechanics (Tiller *et al.*, 1980). For the case of charged colloidal particles this local compressive drag pressure can be related to the local disjoining pressure

$$p_S(D) \equiv p_D(D). \tag{54}$$

This relationship determines the interparticle spacing throughout the filter cake. Further, for particles in a hexagonal close-packed geometry the local particle volume fraction (or voidage) may be related to the interparticle spacing:

$$\phi = 1 - \varepsilon = \frac{V_p}{V} = \frac{4\sqrt{2}}{3}\pi\frac{(a+d)^3}{(2a+D)^3} \tag{55}$$

which could be used to calculate the local specific resistance by the Carman–Kozeny equation (Carman, 1938). For spherical particles this gives

$$\alpha = \frac{45}{(a+d)^2}\frac{(1-\varepsilon)}{\rho_p \varepsilon^3}. \tag{56}$$

Hence, ε (or α) is a function of the disjoining pressure and may be calculated from the preceding fundamental analysis of interparticle interactions. In effect this is a fundamental theory of a type of compressible cake filtration.

The compressive drag force in the filter cake varies from a minimum of zero at the cake–dispersion interface to a maximum at the membrane surface. The actual compressive drag pressure, p_S, can be expressed as a function of the difference between the hydraulic pressure at the cake–dispersion interface, p_1, and that at a depth y, with $0 \leqslant y \leqslant L$, in the cake, p_y, Fig. 5. Thus, since the local cake voidage, ε_y, and the local specific cake resistance, α_y, at any point are functions of the local compressive drag pressure at that point, ε_y and α_y are functions of $(p_1 - p_y)$ with $p_1 \geqslant p_y \geqslant p_2$. The voidage thus decreases from the cake–dispersion interface to the membrane and the resistance shows a corresponding increase.

Membrane ultrafiltration is a dynamic process, which means that the membrane resistance has a significant hydraulic resistance compared to the filter cake resistance, at least at the initial stages of the filtration. This means that the filter cake increases in thickness and resistance as filtration proceeds, so that the ratio of cake resistance to membrane resistance, and hence the ratio of pressure drop across the cake to pressure drop across the membrane, is increasing continuously and therefore a function of time.

Starting with D'Arcy's law for flow of liquids through porous media, and in particular the application to streamline flow through pores in a bed of spherical particles (Kozeny, 1927), it is possible to write the differential expression

$$\frac{1}{A_m}\frac{\mathrm{d}V}{\mathrm{d}t} = \frac{K}{\mu}\frac{\mathrm{d}p_y}{\mathrm{d}y} = \frac{1}{45}\frac{a^2\varepsilon_y^3}{\mu(1-\varepsilon_y)^2}\frac{\mathrm{d}p_y}{\mathrm{d}y} \tag{57}$$

which relates the small element of cake thickness, $\mathrm{d}y$, to the small volume of permeate, $\mathrm{d}V$, passing through its formation, Fig. 5.

However, Happel (1958) developed a rigorous theoretical treatment for flow through porous media

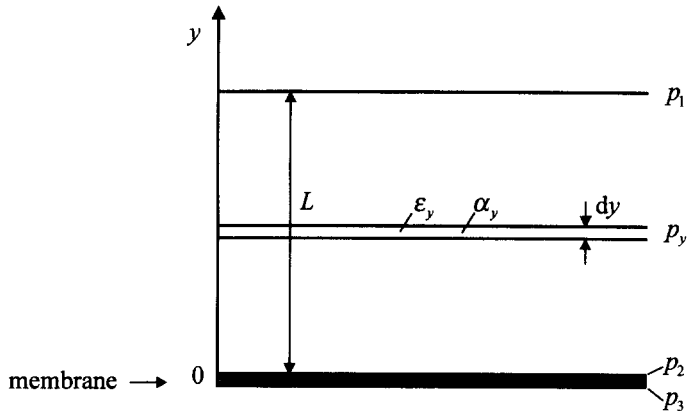

Fig. 5. Schematic diagram of a compressible filter cake.

based on a cell model approach which relaxes the semi-empirical Kozeny approximation, eq. (57). The cell approach applies best where symmetry of the particle assemblage (packing geometry) is more or less complete (Happel and Brenner, 1973). Hence, it is of great application in concentrated particle systems. Happel (1958) obtained a closed solution for the pressure drop per unit length of a packed bed due to passage of fluid through it. The resulting equation was essentially D'Arcy's equation, which provided a theoretical basis for the experimentally derived law. For a hexagonal close-packed particle geometry the equation reads in differential form as follows:

$$\frac{1}{A}\frac{dV}{dt} = \frac{K_{\text{Happel}}}{\mu}\frac{dp_y}{dy} = \frac{1}{\mu}\left(\frac{2a^2}{9(1-\varepsilon)} \times \frac{3 - 4.5(1-\varepsilon)^{1/3} + 4.5(1-\varepsilon)^{5/3} - 3(1-\varepsilon)^2}{3 + 2(1-\varepsilon)^{5/3}}\right)\frac{dp_y}{dy}. \tag{58}$$

Equation (58) is valid over the entire concentration range $\varepsilon = 0.26$–1 and is correlated extremely well with the semi-empirical Kozeny equation [eq. (57)] in the range where the latter is valid ($\varepsilon = 0.26$–0.8). In addition, the cell model proved to be excellent in the high porosity limit, where the Kozeny equation breaks down (Happel, 1958). Hence, eq. (58) will be used in the present work.

As the filter cake is compressible, the volume of cake deposited by the flow of unit volume of permeate will not be constant, but the mass of solids will be almost independent of the conditions under which the cake is formed. A mass balance over the filter cake gives

$$dm_p = c_b\, dV_{\text{Tot}} = c_b\, d(V_{\text{Liq}} + V_{\text{Coll}}) = c_b[dV_{\text{Liq}} + (1-\varepsilon_y)A_m\, dy] \equiv (1-\varepsilon_y)\rho_p A_m\, dy \tag{59}$$

Substituting eq. (59) into eq. (58) and rearranging then gives

$$\frac{1}{A_m}\frac{dV}{dt} = \frac{K_{\text{Happel}}}{\mu}A_m(1-\varepsilon_y)(\rho_p/c_b - 1)\frac{dp_y}{dV} = \frac{K_{\text{Happel}}}{\mu}A_m(1-\varepsilon_y)(\rho_p/c_b - 1)\frac{(-dp_S)}{dV} \tag{60}$$

where use is made of the relationship $dp_y = dp_L = -dp_S$ [see eq. (53)]. Separating the variables and integrating throughout the total volume of the cake (or total permeate volume) gives

$$\int_0^V \frac{dV}{dt}dV = V\frac{dV}{dt} = -A_m^2\left(\frac{\rho_p}{c_b} - 1\right) \times \int_{p_2}^{p_1} \frac{[1-\varepsilon(p_S)]K_{\text{Happel}}(p_S)}{\mu_a(p_S)}dp_S \tag{61}$$

where use is made of the assumption that dV/dt is constant at any instant throughout the cake, which is true when the amount of liquid gained by the compression of the cake at that instant is negligible. Since electroviscous effects in the filter cake are accounted for by the dynamic model, the fluid viscosity is replaced by the apparent fluid viscosity [eq. (47)], which is a function of the compressive drag pressure [via eq. (48)] and therefore appears within the pressure integral of eq. (61).

Equation (61) is a key equation in the development of the dynamic model, together with an equation describing the flux through the membrane,

$$\frac{1}{A_m}\frac{dV}{dt} = \frac{\Delta p_m}{\mu R_m} = \frac{p_2 - p_3}{\mu R_m}. \tag{62}$$

Here, the fluid viscosity has not to be altered due to electroviscous effects, since the membrane resistance is constant and determined experimentally.

The numerical solution of the governing equations can now be undertaken through the adoption of a stepping schema, Fig. 6. The basic concept is that at each time step a new layer of constant specific resistance is formed on top of the membrane surface (due to the accumulation of particles at the open cake surface), the resistance of which is a function of the compressive drag pressure at that point and that time. These local specific resistances (or voidage) are calculated from the preceding interparticle interaction approach. Since $p_2(t)$, the hydraulic pressure at the

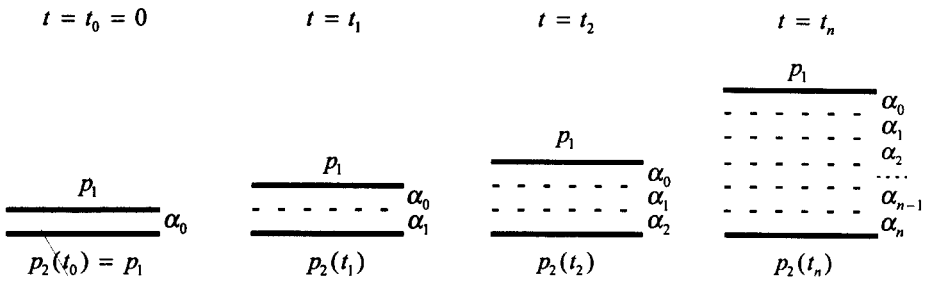

Fig. 6. Schematic description of the time stepping procedure applied in the dynamic ultrafiltration model. α_0 is the initial specific resistance due to the dispersion, i.e. the particle bulk concentration. Flow is from top to bottom in the figure.

membrane surface, is a function of time, by substituting $p_S = [p_1 - p_2(t)]$ and renewing the integral boundaries, eq. (61) can be written,

$$V\frac{dV}{dt} = -A_m^2\left(\frac{\rho_p}{c_b} - 1\right) \times \int_{p_1 - p_2(t)}^{0} \frac{(1 - \varepsilon(p_2(t)))K_{\text{Happel}}(p_2(t))}{\mu_a(p_2(t))}(-dp_2(t)) = A_m^2\left(\frac{\rho_p}{c_b} - 1\right)\int_t^0 \frac{(1 - \varepsilon(t))K_{\text{Happel}}(t)}{\mu_a(t)}\frac{dp_2(t)}{dt}dt \quad (63)$$

and differentiation then gives,

$$\left(\frac{dV}{dt}\right)^2 + V\frac{d^2V}{dt^2} = -A_m^2\left(\frac{\rho_p}{c_b} - 1\right) \times \frac{(1 - \varepsilon(t))K_{\text{Happel}}(t)}{\mu_a(t)}\frac{dp_2(t)}{dt}. \quad (64)$$

Equation (62) can also be differentiated with respect to time:

$$\frac{dp_2(t)}{dt} = \frac{\mu R_m}{A_m}\frac{d^2V}{dt^2} \quad (65)$$

which on substitution into eq. (64) and using the substitution $z = dV/dt$ results in a set of two first-order differential equations and an algebraic equation, which can be solved simultaneously to yield the permeate volume (or flux) as a function of time:

$$\frac{dz}{dt} = -\frac{z^2}{V + A_m R_m\left(\frac{\rho_p}{c_b} - 1\right)(1 - \varepsilon)\left(\frac{\mu}{\mu_a}\right)K_{\text{Happel}}} \quad (66)$$

$$\frac{dV}{dt} = z \quad (67)$$

$$p_2(t) = \frac{\mu R_m}{A_m}z + p_3. \quad (68)$$

The boundary conditions of this dynamic compressible cake ultrafiltration model are:

at $t = 0$, $V = 0$

$p_2(t) = p_1$

$$z = \frac{dV}{dt} = \frac{A_m}{\mu R_m}(p_1 - p_3).$$

The initial cake voidage is given by the "voidage" due to the dispersion, that is, a particle spacing corresponding to the bulk concentration. The dynamic model was solved by a numerical predictor–corrector schema.

3.2. *Theoretical dynamic model predictions*

In this section the dynamic model will be used to explore the effect of zeta-potential, ionic strength, particle radius, membrane resistance and applied pressure on the rate of filtration of monodisperse spherical silica colloids immersed in a sodium chloride electrolyte. In each case one of these parameters will be varied while keeping the others constant at values of practical application. These reference conditions are: $\zeta = 50\,\text{mV}$, $I = 0.01\,\text{M}$, $a = 20\,\text{nm}$, $R_m = 2 \times 10^{13}\,\text{m}^{-1}$ and $\Delta p = 50\,\text{kPa}$. Calculations are presented for a filtration time of 4 h, a bulk particle concentration of $4\,\text{g l}^{-1}$, a temperature of 20°C and a membrane area of $1\,\text{m}^2$. In each case the results are presented as plots of t/V ("reciprocal total filtration rate") vs V, as is common practice for cake filtration. For illustration purposes the classical constant pressure filtration model (Carman, 1938)

$$\frac{t}{V} = \frac{\mu c_b \alpha_{av}}{2A_m^2 \Delta p}V + \frac{\mu R_m}{A_m \Delta_p} \quad (69)$$

with an average constant specific cake resistance, i.e. at close-packed condition, is compared with the dynamic model where appropriate.

Figure 7 shows the effect of varying the zeta-potential in the range 0–100 mV. The line of the classical filtration model is the limiting case for close-packed particles with no particle–particle interactions considered. Increase in the magnitude of ζ gives much faster rates of filtration as the particles are forced apart and the specific resistance of the cake decreases. These changes are especially marked in the range $\zeta = 0$–$50\,\text{mV}$. A plot of t/V vs V is expected to be linear for an incompressible cake. All of the predicted lines in Fig. 7 are curved due to the cake compressibility, with an approach to linearity as filtration proceeds and the cake resistance increases so that the

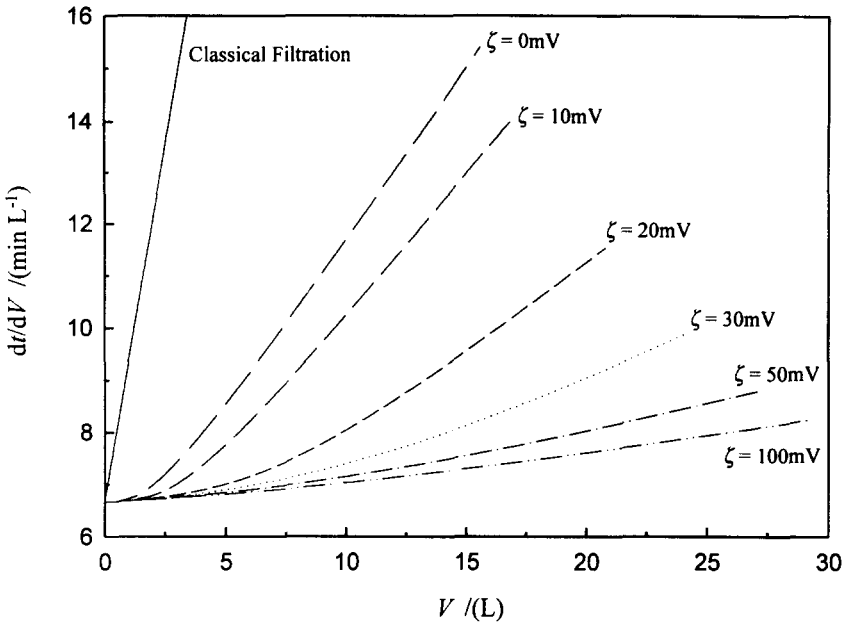

Fig. 7. Effect of zeta-potential on the reciprocal filtration rate. Model parameters as given in text.

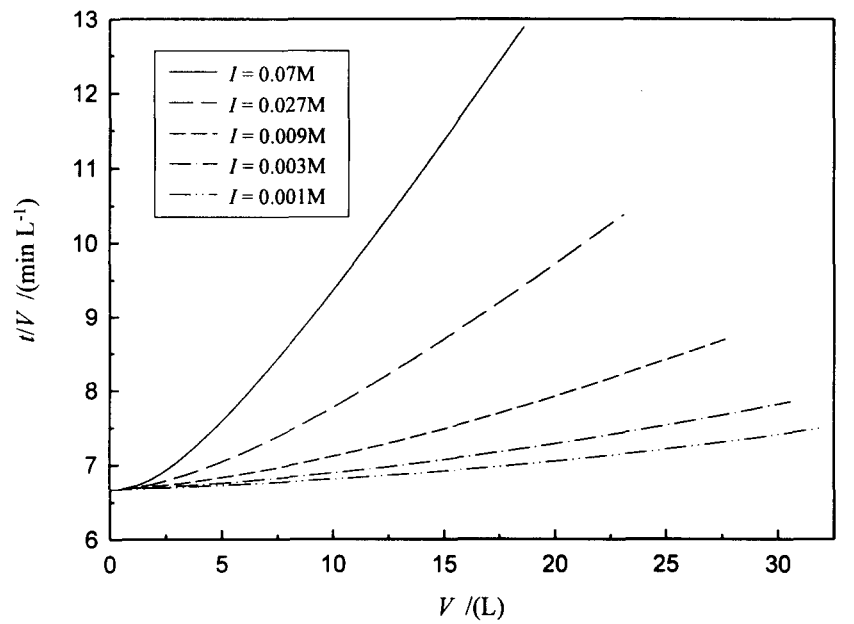

Fig. 8. Effect of ionic strength on the reciprocal filtration rate. Model parameters as given in text.

membrane resistance becomes negligible. Figure 8 shows the effect of varying the ionic strength in the range 0.001–0.07 M. Decreasing the ionic strength gives greater overall rates of filtration and greater curvature to the plots, as the double layer extent in solution (Debye-length) increases preventing close approach of the particles and resulting in lower specific resistances.

The predictions for particles with radii in the range 5–150 nm are shown in Fig. 9. Also shown in the figure are the "limiting results" resulting from the assumption of close packing and the neglect of particle–particle interactions (classical filtration model). Even for particles of radius 150 nm there is a discrepancy between the predictions of the dynamic model and the limiting result. This discrepancy increases substantially as the particle size is decreased, and for particles of radius 5 nm neglect of interparticle interactions leads to serve underprediction of filtration rates. Thus, interparticle interactions are significant

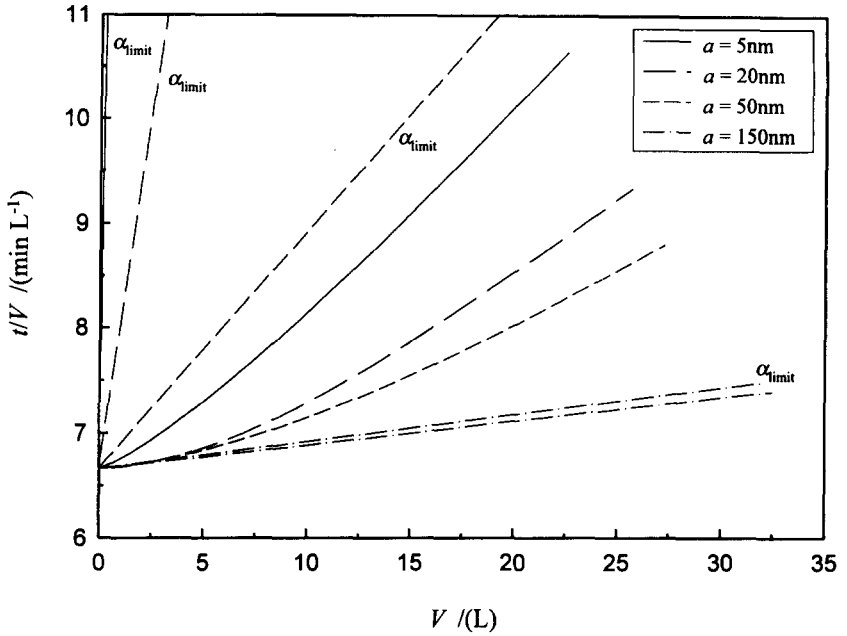

Fig. 9. Effect of particle radius on the reciprocal filtration rate. Model parameters as given in text.

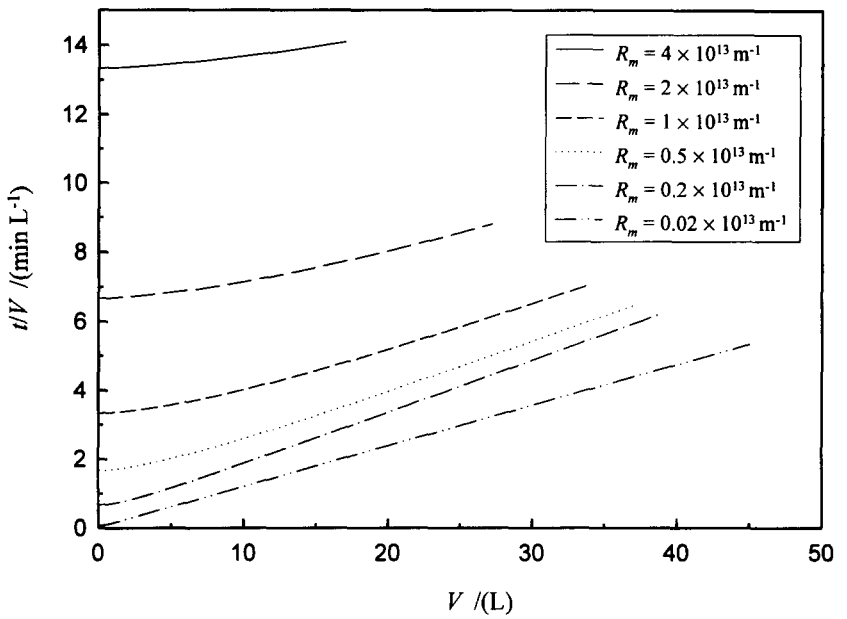

Fig. 10. Effect of membrane resistance on the reciprocal filtration rate. Model parameters as given in text.

even for particles in the microfiltration range and become very important in the true ultrafiltration range.

The dynamic model also predicts the effect of parameters which are not direct properties of the particles being filtered. Thus, Fig. 10 shows the effect of variation of the membrane resistance, R_m, in the range 0.02×10^{13}–$4 \times 10^{13}\,m^{-1}$. As the membrane resistance becomes higher so the filtration rate decreases and the initial curvature in the plots becomes more pronounced. For comparison, resistances of 2×10^{13} and $0.4 \times 10^{13}\,m^{-1}$ correspond, respectively, to polyethersulphone NADIR ultrafiltration membranes (Hoechst AG, Germany) of molecular weight cut-off (MWCO) 4000 and 30,000, respectively. A membrane of resistance $0.02 \times 10^{13}\,m^{-1}$, for which no substantial initial curvature in the plots is predicted, might well be inside the microfiltration range. Finally, Fig. 11 shows the effect of variation of the applied pressure in the range 25–400 kPa. As expected, filtration rates in-

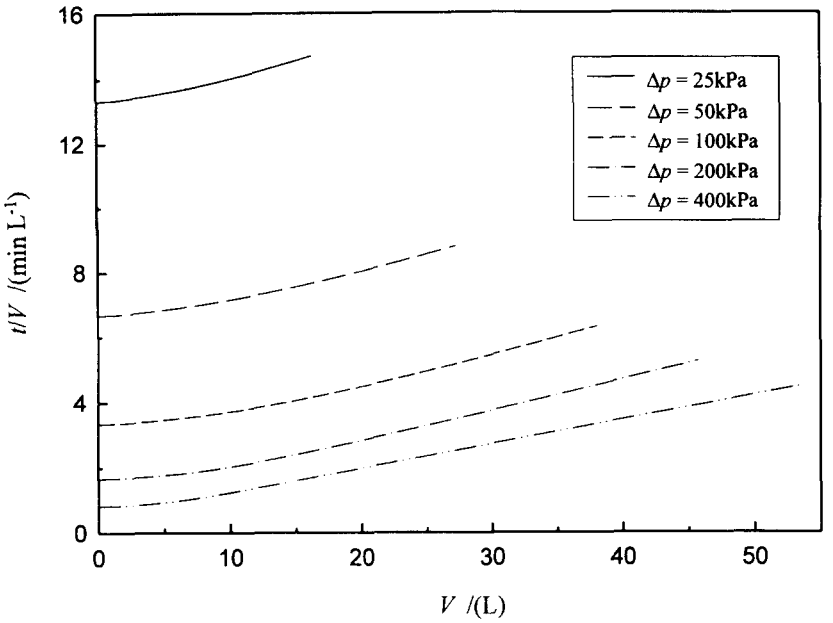

Fig. 11. Effect of applied pressure on the reciprocal filtration rate. Model parameters as given in text.

crease as the applied pressure is increased. However, the dynamic nature of the ultrafiltration process is most pronounced at low pressure.

To reveal the effect of the disjoining pressure components, i.e. electrostatic, van der Waals, hydration and configurational entropy, on the dynamic ultrafiltration model predictions, theoretical calculations for the same colloidal silica system have been performed under the following extreme and intermediate conditions:

(1) $I = 0.001\,\mathrm{M}$, $\zeta = 120\,\mathrm{mV}$,

(2) $I = 0.006\,\mathrm{M}$, $\zeta = 100\,\mathrm{mV}$,

(3) $I = 0.03\,\mathrm{M}$, $\zeta = 50\,\mathrm{mV}$,

(4) $I = 0.07\,\mathrm{M}$, $\zeta = 10\,\mathrm{mV}$.

The other input parameters are constant and as follows: $a = 20\,\mathrm{nm}$, $\Delta p = 50\,\mathrm{kPa}$, $R_m = 2 \times 10^{13}\,\mathrm{m}^{-1}$. The filtration time is 10 h, the particle bulk concentration is $4\,\mathrm{g\,l}^{-1}$, the temperature is 293.15 K and the membrane area is $1\,\mathrm{m}^2$.

Figure 12(a) clearly indicates the overwhelming effect of the repulsive electrostatic pressure at low ionic strength (and high zeta-potential), where the electrical double layer extent, i.e. the Debye-length, is large. The other disjoining pressure contributions are more or less negligible. After 10 h of filtration simulation the final particle–particle separation in the filter cake (first layer above the membrane surface) is equal to 15.1 nm, which indicates a highly porous cake. Increasing the ionic strength and hence decreasing the zeta potential (at constant pH) reduces the Debye-length and the other pressure terms become more effective, Fig. 12(b)–(d). In particular, it can be seen that the disjoining entropic pressure has a comparable influence to the electrostatic pressure at higher ionic strength. This was not clear *a priori*, since the configurational entropic term scales with the inverse of the cubed particle radius and seemed to be negligible for the relatively large investigated particle size ($a = 20\,\mathrm{nm}$). However, the final particle–particle approach is 8.91 nm [Fig. 12(b)] and 3.06 nm [Fig. 12(c)] and the filter cake gets more and more compressed. At high ionic strength [Fig. 12(d)] the electrostatic force is substantially screened by the double layer ions and has only a secondary impact on the total disjoining pressure. The final particle separation is 1.35 nm, which is near to close-packed conditions ($D = 1.1\,\mathrm{nm}$).

It can be seen from all four figures that the disjoining hydration pressure has a short decay length, but rises very steeply at close packed conditions. The hydration pressure therefore prevails at very small-particle separations and is the dominant repulsive contribution. The attractive van der Waals contribution seems to be small, but this is due to the relatively low Hamaker constant of the silica system. The insets in all four figures display the electroviscous effects as a function of the interparticle spacing. The apparent viscosity is highest, of course, for low electrolyte concentrations and high zeta-potentials.

Figure 13 visualises the effect of the hydration forces, the electroviscous effects and the configurational entropy in terms of a filtration analysis plot, t/V vs permeate volume. Again, including hydration forces predicts an increased filtration rate only a high ionic strength where the particles are nearly close-packed, whereas the electroviscous effect is at its greatest at low ionic strength and high zeta-potential, reducing the rate of filtration. The configurational entropic pressure has quite an influence on the filtration rate

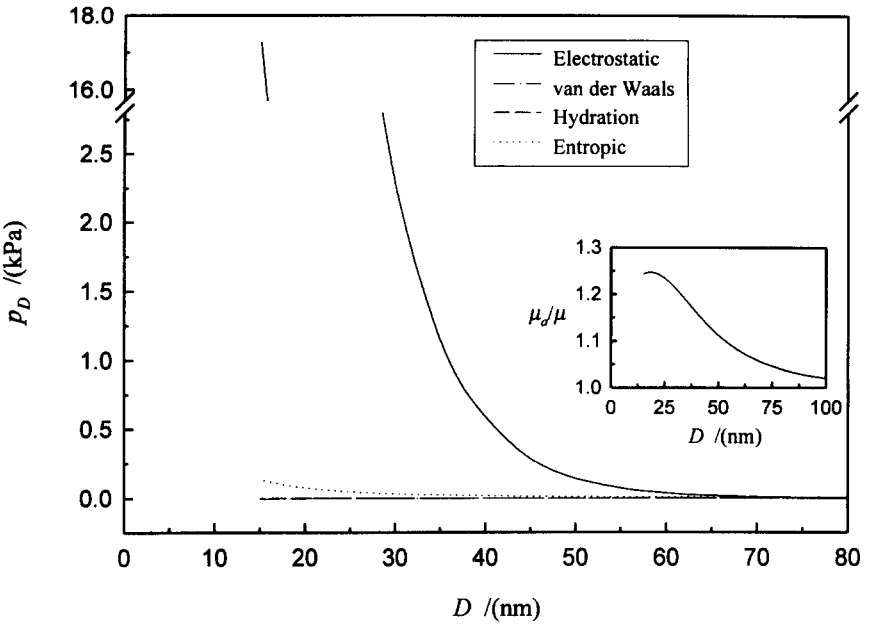

Fig. 12(a). Disjoining pressures vs interparticle distance for $I = 0.001$ M and $\zeta = 120$ mV. Final particle separation in the filter cake after 10 h of filtration is 15.1 nm.

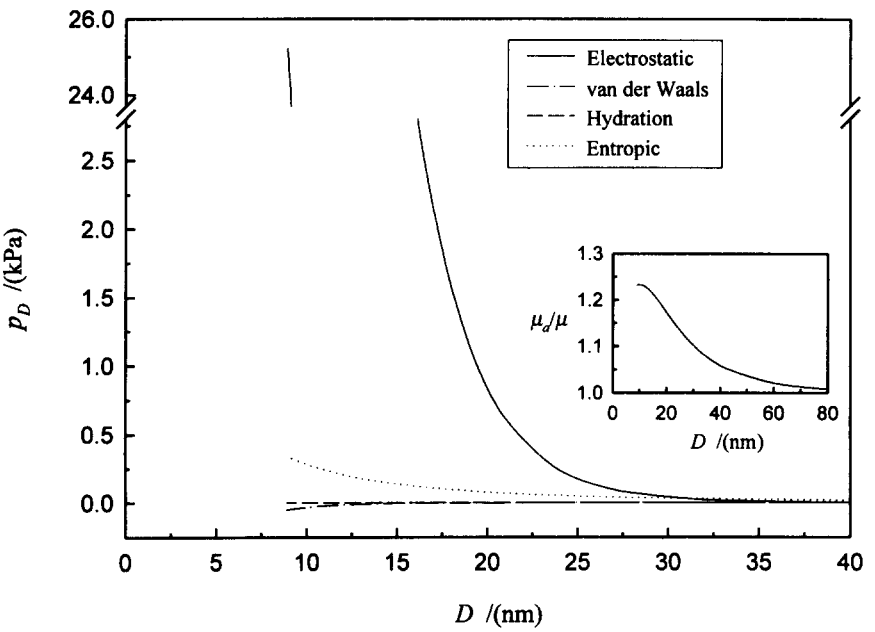

Fig. 12(b). Disjoining pressures vs interparticle distance for $I = 0.006$ M and $\zeta = 100$ mV. Final particle separation in the filter cake after 10 h of filtration is 8.91 nm.

extending even to low electrolyte concentrations. This is specifically true at the initial stages of the theoretical filtration runs, since the configurational entropy contribution, although it is quite modest, has a large "decay length" which makes it the dominant contribution at large interparticle distances [Fig. 12(c) and (d)]. At intermediate electrolyte concentration both the electroviscous effects and the entropic pressure are significant. The lines for the case "without electroviscous effects" are visually missing for the highest ionic strength in Fig. 13, as are the lines for the case "without hydration forces" for the two lowest ionic strengths, as they are coincident with the dynamic cell model lines.

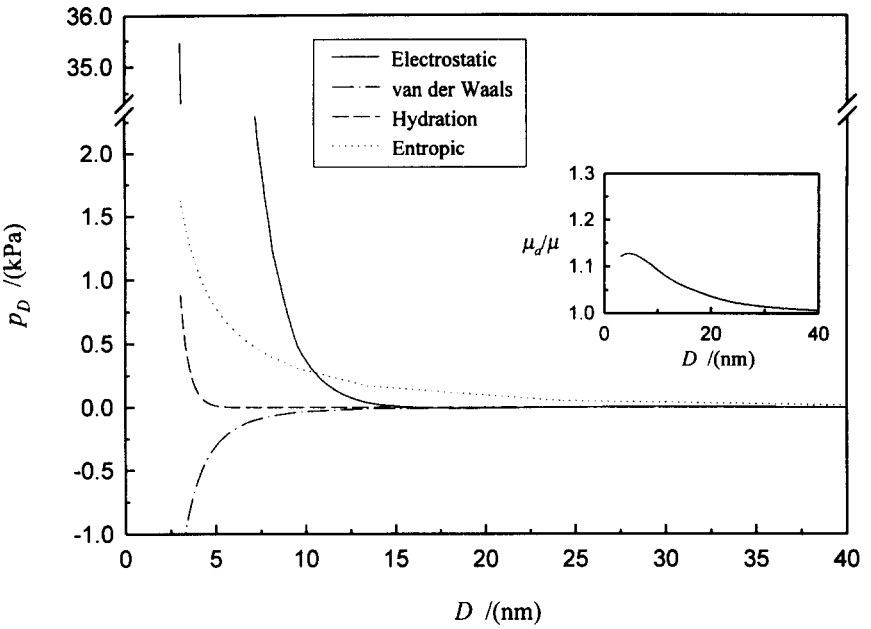

Fig. 12(c). Disjoining pressures vs interparticle distance for $I = 0.03$ M and $\zeta = 50$ mV. Final particle separation in the filter cake after 10 h of filtration is 3.06 nm.

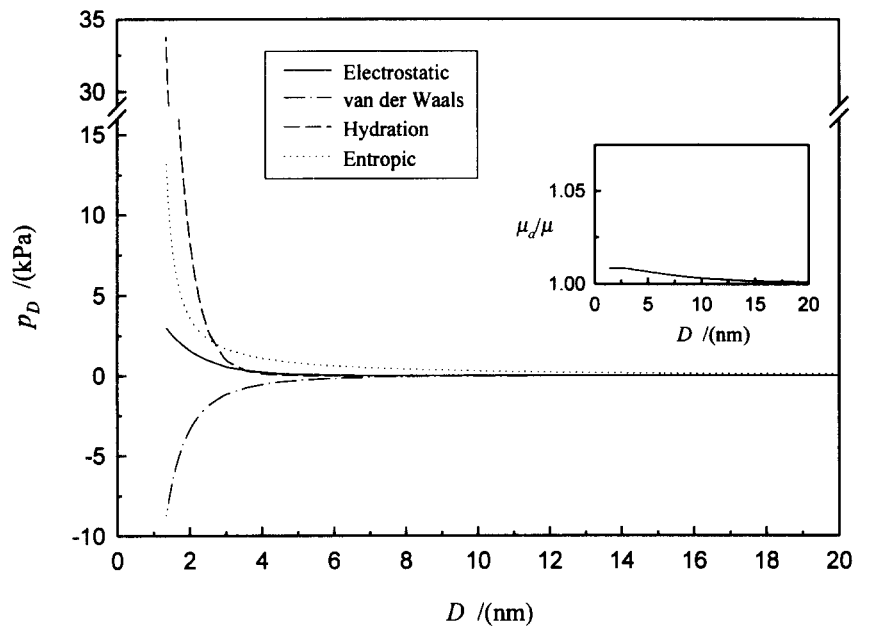

Fig. 12(d). Disjoining pressures vs interparticle distance for $I = 0.07$ M and $\zeta = 10$ mV. Final particle separation in the filter cake after 10 h of filtration is 1.35 nm.

4. COMPARISON OF THE DYNAMIC MODEL AND EXPERIMENT

4.1. *Experimental materials and procedures*

The predictions of the dynamic model have been compared to experimental results for the filtration of monodisperse spherical silica colloids (Syton W30, Monsanto) with variation of zeta-potential (through change of pH) and ionic strength to give a variation of the particle properties. The particle size was determined by photon correlation spectroscopy using an AutoSizer Lo-C (Malvern Instruments, UK) equipped with an Uniphase 75 mW Argon laser. The mean particle radius was found to be 24.3 ($\pm$2.3) nm for all conditions reported. Electrophoretic mobility measurements were made using a ZetaMaster (Malvern Instruments, UK). Electrophoretic mobility values

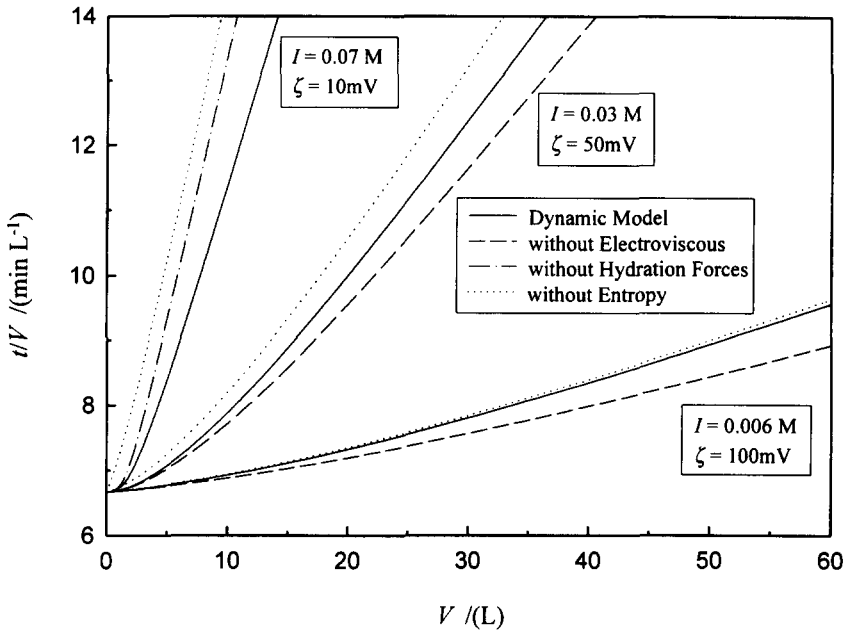

Fig. 13. Dynamic model approach with and without electroviscous effects, hydration forces and configurational entropy. The line for the case "without electroviscous effects" is visually missing for the highest ionic strength, as are the lines for the case "without hydration forces" for the two lowest ionic strengths, as they are coincident with the dynamic cell model lines.

were converted to zeta-potential using the WinMobil programme (Department of Mathematics, University of Melbourne) which is an extended implementation of an advanced theory of electrophoresis (O'Brien and White, 1978).

Ultrafiltration measurements were carried out using a 50 ml filtration cell (Amicon Corporation, model 8050) connected to a solution reservoir with a maximum capacity of 250 ml. The effective membrane area was 13.4 cm^2. The system was pressurised using nitrogen gas. The cell was not stirred. The temperature was maintained constant at 20 °C. The filtration time was coupled to the amount of permeate collected, i.e. it was stopped after 30 ml were collected. The total filtration time was therefore in the range 3–6.5 h, depending on the ionic concentration and zeta-potential conditions. Rates of filtration were determined by continuously weighing the filtrate on an electronic balance connected to a microcomputer. The electrolyte used was NaCl with variation of pH by addition of NaOH and HCl. NADIR polyethersulphone membranes of molecular weight cut-off 4000D (Hoechst AG, Germany) were used. The hydraulic resistance of the membrane discs used was in the range $2.05–2.30 \times 10^{13}\ m^{-1}$.

Each experimental run (for different dispersions) has been repeated several times and high reproducibility was achieved. Using the same colloidal dispersion and the same membrane (rinsed after each run, where the pure electrolyte flux was always established again) a relative experimental error band width of less than $\pm 1.5\%$ compared to the average value at 30 ml on a t/V vs V plot could be affirmed.

Unfortunately, no previously published experimental filtration data give sufficient experimental detail for a rigorous comparison with the present theoretical predictions. However, in those cases where it was possible to estimate omitted experimental details (which were few), such previous data were in good agreement with the present predictions.

4.2. *Experimental results and model predictions*

Figure 14(a)–(g) give filtration data showing the effect of variation of zeta-potential at constant ionic strength and applied pressure ($I = 0.03$ M, $\Delta p = 50$ kPa). The zeta-potential was varied in the range $-5.3 - -92.6$ mV by varying the pH in the range 3.0–9.0. In addition to the experimental data, each plot shows the predictions of the dynamic ultrafiltration model. The limiting case predictions [classical filtration model, eq. (69)] if interparticle interactions are neglected and close-packing of particles is assumed are also shown. The scaling of the t/V axes has been adjusted to improve visualisation of the varying effects.

These figures clearly reveal the excellent quantitative predictive ability of the developed rigorous dynamic ultrafiltration model for colloidal dispersions over the whole pH or zeta-potential range. It should be noted that the model predictions are physics-based with no adjustable parameters. Hence, the dynamic cell model can predict all possible stages of interparticle separations within the filter cake as a function of the filtration time-dependent pressure difference across the cake. The figures illustrate that the dynamic model includes properly all the governing physical

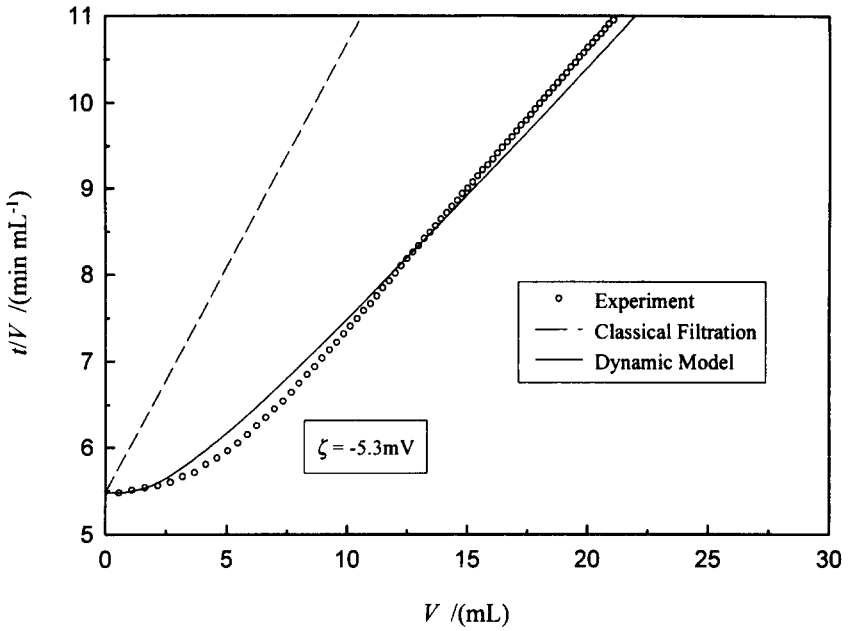

Fig. 14(a). Time over volume vs permeate volume at pH = 3.0, I = 0.0338 M.

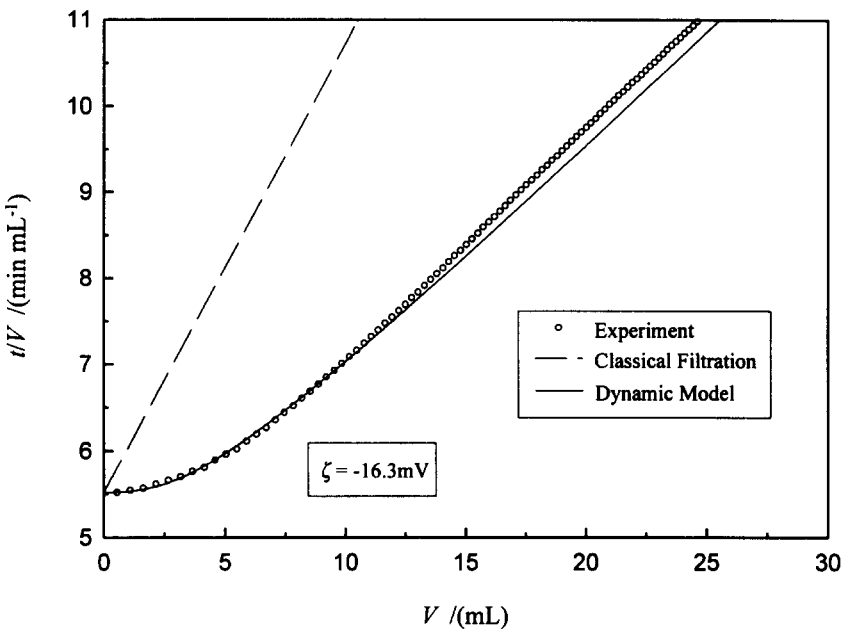

Fig. 14(b). Time over volume vs permeate volume at pH = 4.0, I = 0.0310 M.

effects, which make it such a good predictive description of the colloidal ultrafiltration process. However, the slight overpredictions at high zeta-potentials could arise from the fact that the calculation of the zeta-potential by the O'Brien and White (1978) theory from the electrophoretic mobility measurements is subject to uncertainty at very high zeta-potential. If the O'Brien and White (1978) predictions are overestimating the real zeta-potential, as it is believed, then the filtration rate predictions will also be overestimates. However, for all experimental conditions the classical filtration model, i.e. a neglect of interparticle interactions, gives a very substantial underestimation of the filtration rate.

Figure 15(a)–(e) gives filtration data showing the effect of variation of ionic strength (I = 0.001–0.07 M) at a constant pH value of 4.0. It should be noted that this also gives a variation in ζ due to the compression of the double layer as the ionic strength is increased. The excellent agreement between the dynamic model

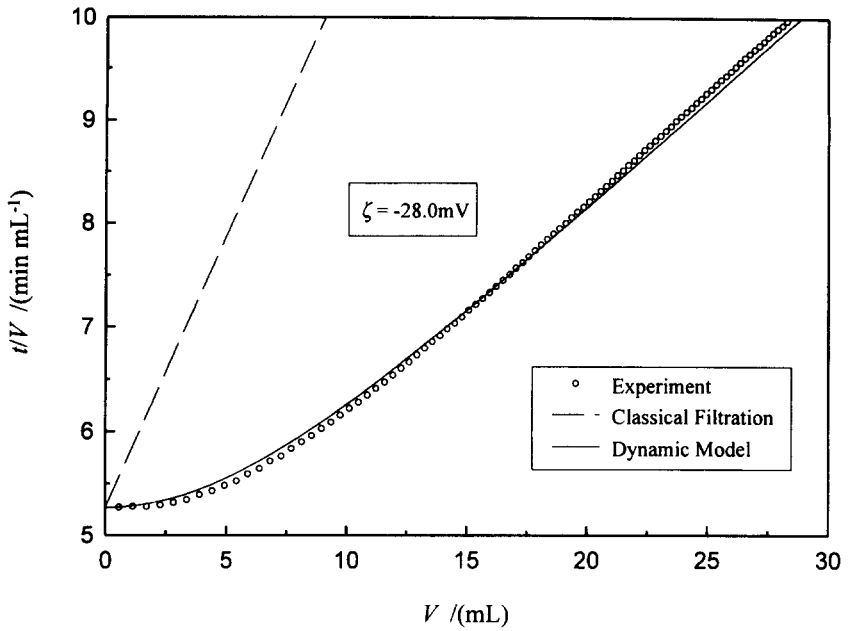

Fig. 14(c). Time over volume vs permeate volume at pH = 5.0, I = 0.0302 M.

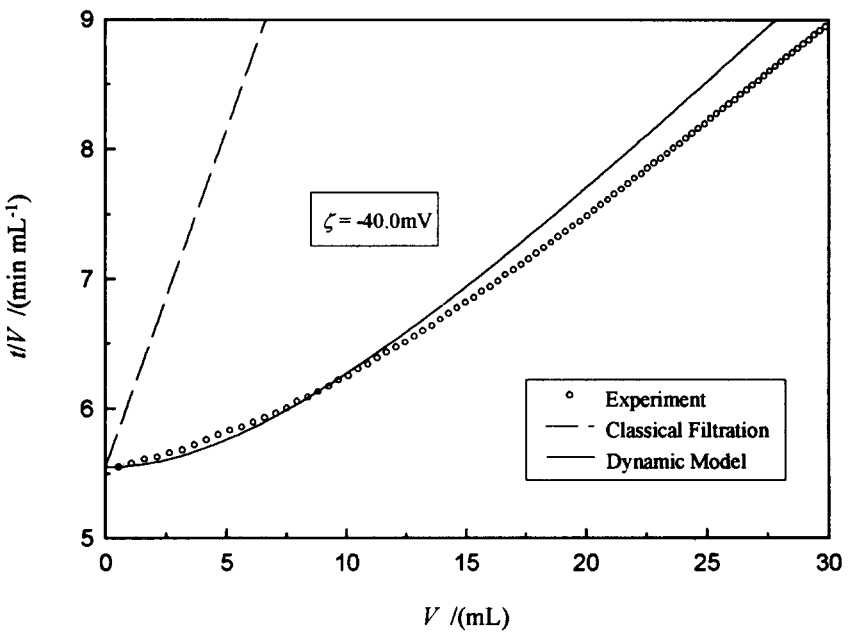

Fig. 14(d). Time over volume vs permeate volume at pH = 6.0, I = 0.0308 M.

and the experimental results is maintained for intermediate ionic strength [Fig. 15(b) and (c)], but the model is underpredicting the experimental filtration rate at high ionic strength [Fig. 15(a)] and overpredicting at low ionic strength (Fig. 15(d) and (e)].

The difference between the experimental filtration result and the dynamic model prediction at high ionic strength, Fig. 15(a), is probably due to the fact that under these ionic conditions (I = 0.07 M, pH 4) the gel-time of the silica particles is reduced to a few hours or even less (Iler, 1979) depending heavily on particle concentration. Since, the filter cake in the present case is near to close-packed, a gelling of the silica particles is quite likely to occur after about 1.25 h. This is in fact indicated by the change in slope in the experimental filtration line in Fig. 15(a). This will lead to an increase in the effective particle size (due to particle aggregation) and hence an increase in filtration rate.

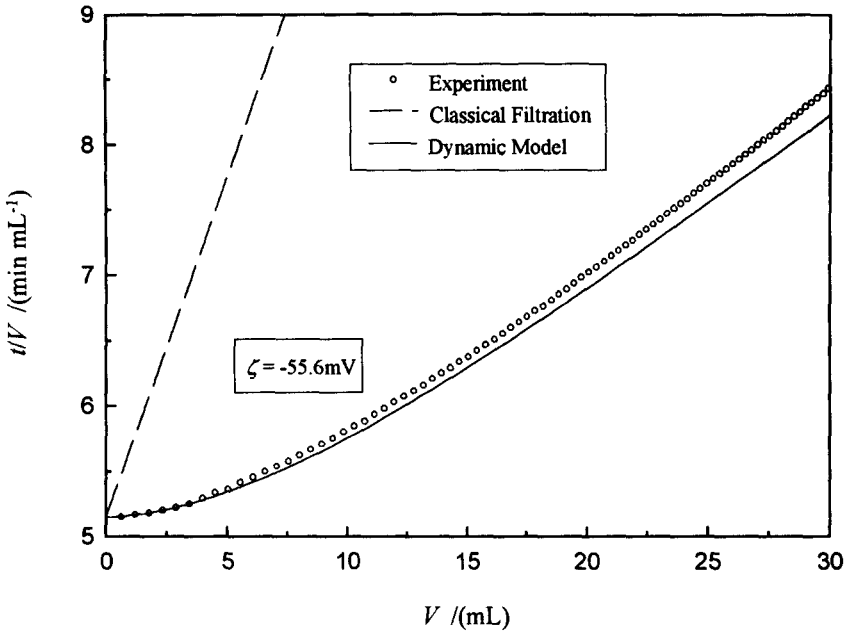

Fig. 14(e). Time over volume vs permeate volume at pH = 7.0, I = 0.0301 M.

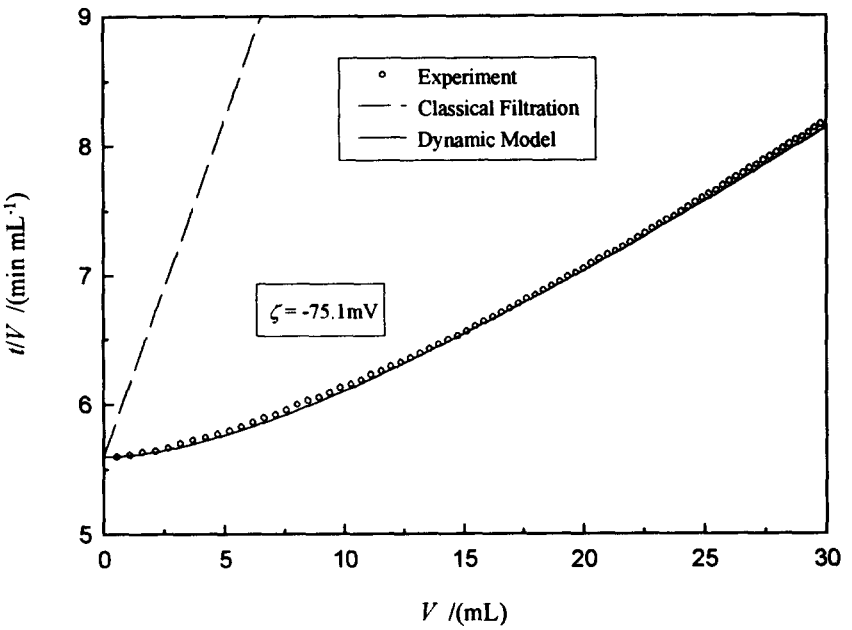

Fig. 14(f). Time over volume vs permeate volume at pH = 8.0, I = 0.0301 M.

The behaviour of the model at low ionic strength is believed to be due to the fact that the calculation of κ, which is based on the ionic concentration in the bulk of the dispersion, is not anymore correct at low electrolyte concentration. Beunen and White (1981) have shown that for concentrated dispersions "connected" to a reservoir of bulk electrolyte the ionic environment within the dispersion is not equal to the bulk electrolyte even though they are in chemical equilibrium. When the particles approach each other there will be a net excess of counterions present at the cell boundary due to the dissociation of the surface charge, which is different to the counterion concentration in the bulk of the solution. Hence, κ should be calculated based on the ion concentration in the reference state to the potential, usually at $\psi = 0$ (i.e. in the bulk of a dilute system), but in a concentrated dispersion there will be no zero-potential point, which means that the reference point has to be at the cell boundary. As mentioned above, the ion concentration

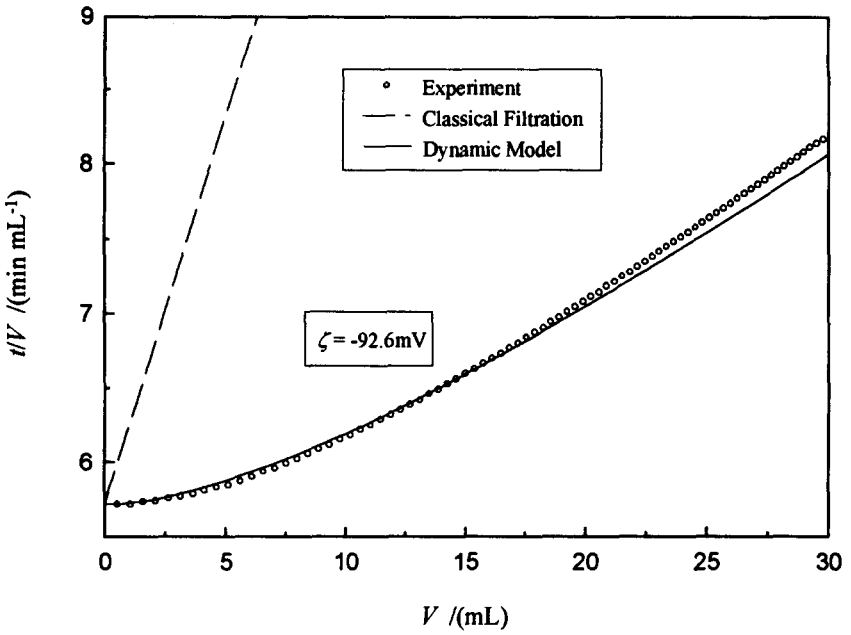

Fig. 14(g). Time over volume vs permeate volume at pH = 9.0, I = 0.0307 M.

will be greater at the cell boundary than in the bulk, which results in a larger κ value and hence in a diminished Debye-length. This will force the particles closer together and reduce the rate of ultrafiltration. The final result is that κ is a function of the interparticle spacing as well, which must then be calculated iteratively with the electrostatic potential at the cell boundary, yielding the disjoining pressure. To realise this a complete charge regulation model of the particle surface would be desirable to give the correct ion concentration when the particles get closer. It is believed that the above-described facts would account for the discrepancy between the filtration rate predictions and the experimental results at low electrolyte concentrations, but usually require detailed information of the surface chemistry of the particles being filtered and also give a substantially increased computing requirement. On the other hand, this shows

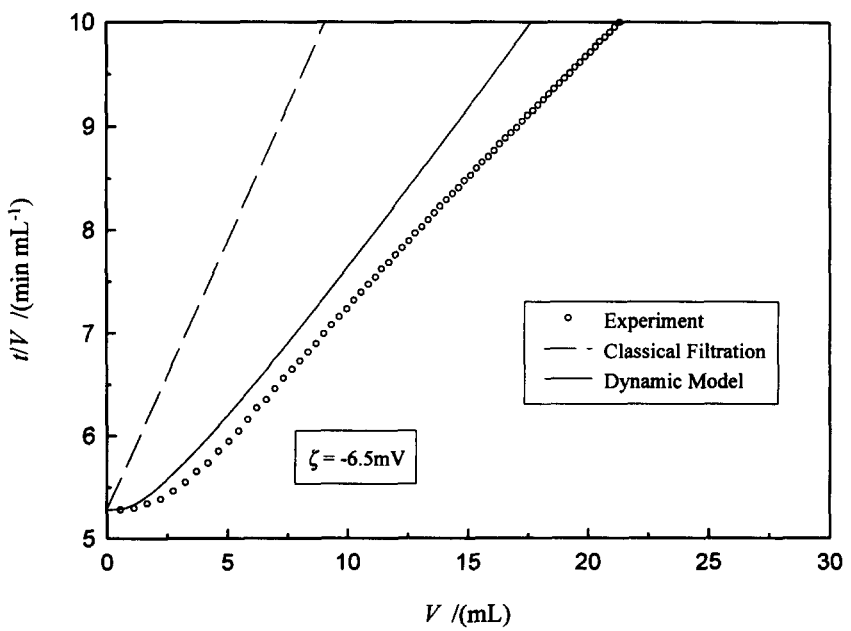

Fig. 15(a). Time over volume vs permeate volume for I = 0.0701 M, pH = 4.0.

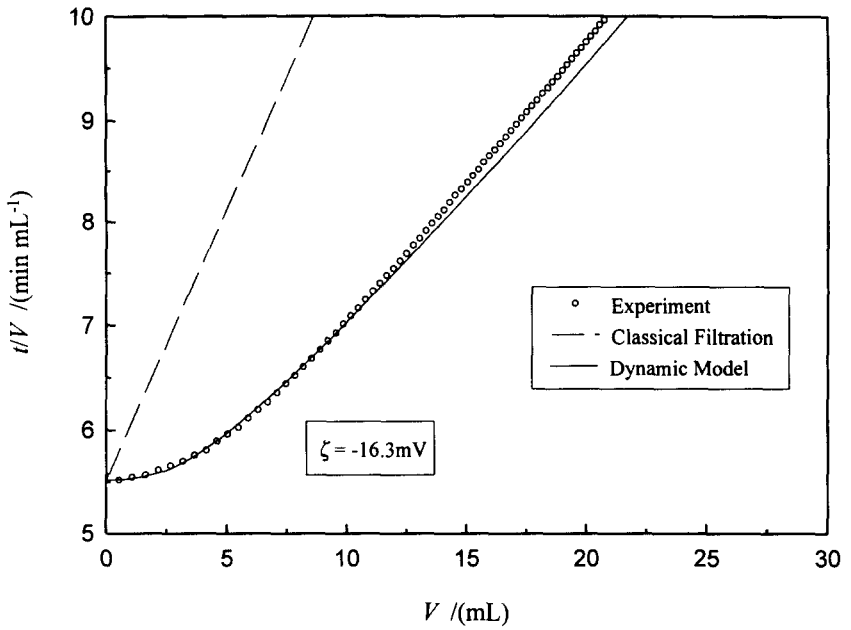

Fig. 15(b). Time over volume vs permeate volume for $I = 0.0310$ M, pH = 4.0.

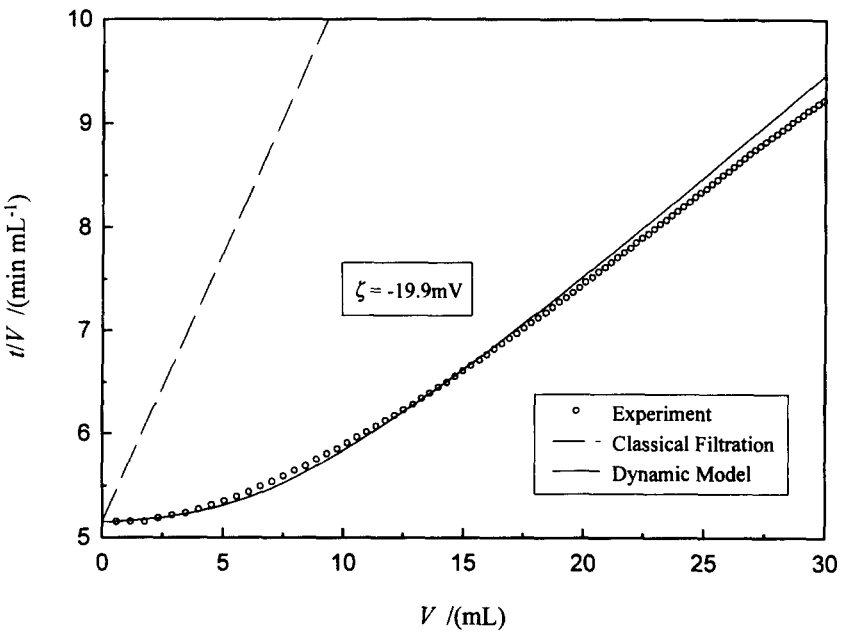

Fig. 15(c). Time over volume vs permeate volume for $I = 0.0108$ M, pH = 4.0.

that the constant zeta-potential approach, as a charge regulation description, is in doubt at low ionic strength. Or, more optimistically, that the simple constant zeta-potential approach is an excellent description for $\kappa a > 1$.

However, the dynamic ultrafiltration model shows excellent predictive performance compared to the classical particle filtration model. The particle–particle interactions in the filter cake, as modelled in the present work, clearly determine the experimental colloidal flux behaviour.

5. CONCLUSIONS

The paper has developed a rigorous mathematical model for predicting the rate of filtration of charged colloidal dispersions based on mathematical descriptions of the particle–particle interactions within filter

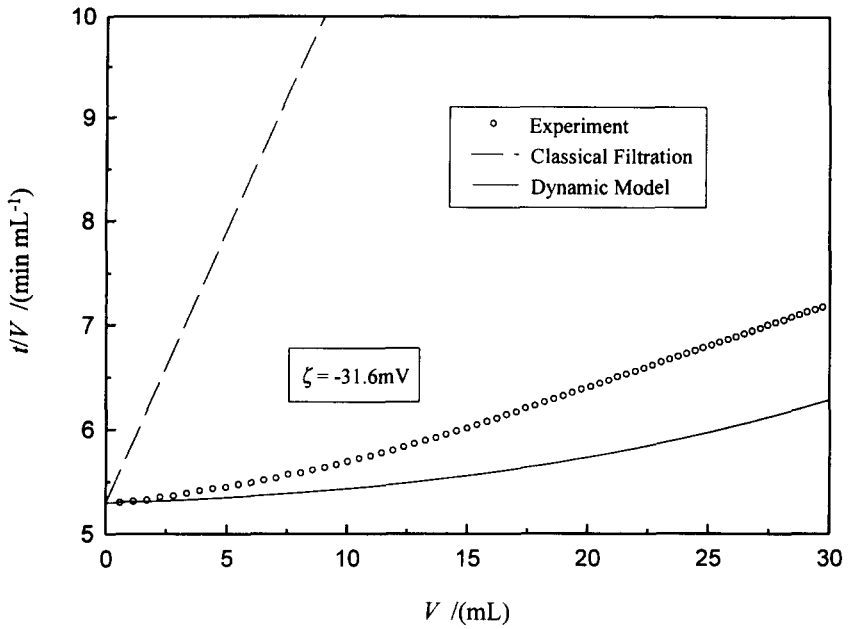

Fig. 15(d). Time over volume vs permeate volume for $I = 0.0033$ M, pH = 4.0.

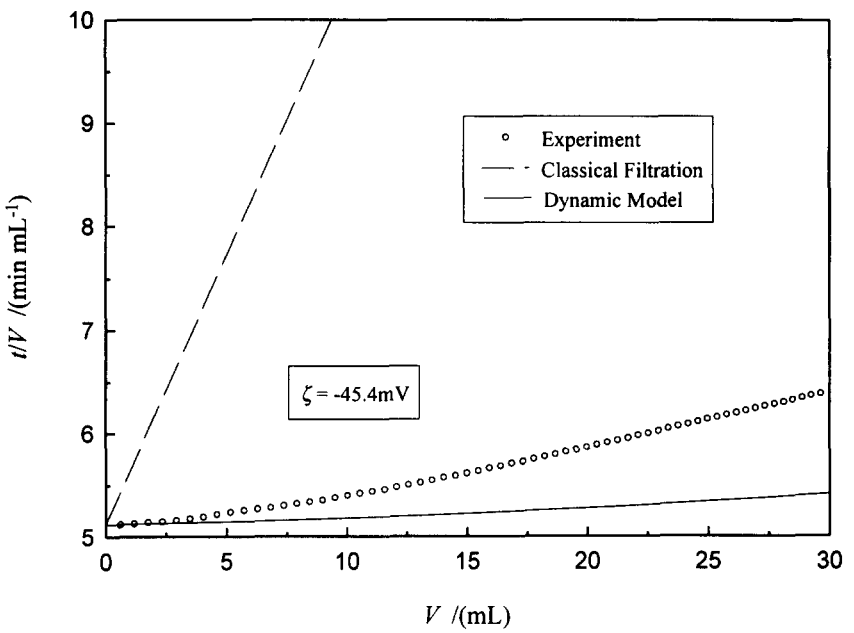

Fig. 15(e). Time over volume vs permeate volume for $I = 0.0010$ M, pH = 4.0.

cakes which are responsible for controlling permeation rates. Each of the types of interaction considered has been quantified in a sophisticated manner. Thus, electrostatic (double layer) interactions have been accounted for by means of a Wigner–Seitz cell approach which includes a solution of the non-linear Poisson–Boltzmann equation. This is known to give excellent agreement with a rigorous finite element solution of the configurational electrostatic interaction energy per particle in a concentrated system. London–van der Waals forces have been calculated using an approximated screened, retarded Lifshitz–Hamaker constant for flat plates with the Hamaker geometrical factor for spheres. This approach is known to give excellent agreement with an exact Lifshitz solution. Hydration forces, for which there is no established fundamental theory, have been included by utilising mathematical expressions derived from the latest results obtained with surface-forces apparatus. Configurational entropy effects have been

calculated using an equation of state which gives excellent agreement with molecular dynamic data. Electroviscous effects have also been accounted for.

These descriptions of particle–particle interactions in assemblages have been used to develop an *a priori* model that allows quantitative prediction of the rate of filtration of charged colloidal dispersions as a function of particle composition, zeta-potential, ionic strength, applied pressure, particle radius and membrane resistance. The model contains no adjustable parameters, it is a calculation "*from physics to filtration*". This is a dynamic model which takes into account the variation of local specific cake resistance as a function of both position in the cake and time. (One feature of the model is, hence, that it may also be considered as providing a fundamental description of a type of compressible cake filtration). The predictions of the model have been systematically investigated. This investigation showed the relative importance of the different types on interaction under different operating conditions and in particular showed the great importance of taking particle–particle interactions into account for ultrafiltration.

The predictions of the model have been compared with experimental results for the filtration of colloidal silica dispersions. There was excellent agreement between theory and experiment for all values of zeta-potential at intermediate ionic strengths. It is especially satisfying that such agreement can be obtained for a model with no adjustable parameters. The excellent agreement is a confirmation of the appropriateness of the descriptions of fundamental interactions included as the basis of the model and of its development to account for the dynamic nature of ultrafiltration. Many practical applications of ultrafiltration occur with feeds with an ionic strength in the range where the model gives such excellent agreement with experiment. Some discrepancy occurs between theory and experiment if aggregation takes place within the filter cake, as can occur at high ionic strength. Deviation between theory and experiment also occurred at low ionic strength. Under such conditions, the ionic strength in concentrated colloidal dispersions depends on the degree of ionisation of the charge-determining surface groups on the colloid surface. Such effects could be included in models of this type if sufficient knowledge of such surface properties was available, but due to the substantial increase in required input parameters (which are often not well-known) and resulting additional computational complexity have not been included in the present work.

Overall, the theoretical work confirms the overwhelming importance of including an account of interparticle interactions in quantitative descriptions of ultrafiltration.

Acknowledgements—We thank the UK Engineering and Physical Sciences Research Council for funding this work. We thank Paul Williams of our Department for the analysis of configurational entropy presented in Section 2.6.

NOTATION

a	Particle radius, m
A	Cross-section area of filter cake, m^2
A_h	area of a hexagon, m^2
A_m	area of membrane surface, m^2
A_H	Hamaker constant (in vacuum), J
A_{ijk}	effective Hamaker constant, J
c_b	particle bulk concentration, $kg\,m^{-3}$
c	velocity of light in vacuum (3×10^8), $m\,s^{-1}$
d	distance [made up from one sodium ion diameter and one hydrated sodium ion radius (Israelachvili, 1991)] of OHP from the particle surface ($=0.55 \times 10^{-9}$), m
D	interparticle distance (surface–surface separation), m
e	elementary charge (1.6×10^{-19}), C
E	electric field strength, $V\,m^{-1}$
f	configurational force, N
F	interparticle force, N
F_S	accumulative drag force on particles, N
G	free energy, J
h	Planck's constant ($=6.625 \times 10^{-34}$), J s
$\hbar$	($=h/2\pi$), $J\,s\,rad^{-1}$
I_s	streaming current (or convective current), A
I_c	conduction current, A
I	ionic strength, $kmol\,m^{-3}$
k	Boltzmann constant (1.38×10^{-23}), $J\,K^{-1}$
K	permeability coefficient, m^{-2}
K''	Kozeny's constant ($=5$, especially for spheres), dimensionless
L	thickness of filter cake, m
m	ionic mobility, $m^2\,s^{-1}\,V^{-1}$
m_p	mass of particles in the cake, kg
$M(R)$	transform function, dimensionless
n	ion number concentration, m^{-3}
n_{0_i}	refractive index, dimensionless
N_A	Avogadro constant (6.0225×10^{26}), $kmol^{-1}$
p	pressure, $N\,m^{-2}$
Δp	pressure difference, $N\,m^{-2}$
$\bar{p}$	osmotic pressure difference, $N\,m^{-2}$
p_S	compressive drag pressure, $N\,m^{-2}$
r	radial coordinate, m
r_c	radius of cylindrical capillary, m
r_{cell}	radius of spherical cell, m
R	interparticle centre–centre distance, m
R	($=\kappa r$) dimensionless radial coordinate, dimensionless
R_c	($=\kappa r_c$), dimensionless
R_m	resistance of membrane, m^{-1}
S_{cell}	surface area of spherical cell, m^2
t	time, s
T	temperature, K
T_i	truncation error per step, dimensionless
ΔT_i	relative truncation error per step, dimensionless
V	total volume filtered, m^{-3}
V_A	attractive interaction energy, J
V_R	repulsive interaction energy, J
V_S	solvent-structural interaction energy, J
V_T	total interaction energy, J

x, y, z Cartesian coordinates, m
z valency, dimensionless

Greek letters

α specific resistance of cake deposit, $m\,kg^{-1}$
α $[=\kappa(a+d)]$, dimensionless
β $(=\kappa r_{cell})$, dimensionless
Δ_i per step spacing between two function evaluations, dimensionless
ε fractional voidage of cake deposit, dimensionless
ε_0 permittivity of vacuum (8.854×10^{-12}), $CV^{-1}m^{-1}$
ε_r dielectric constant, dimensionless
ζ zeta-potential, V
κ Debye–Hückel parameter defined by eq. (12), m^{-1}
μ dynamic viscosity of solvent, $kg\,m^{-1}s^{-1}$
ξ reduced zeta-potential $[=ze\zeta/(kT)]$, dimensionless
Π osmotic pressure of ions inside the double layer, $N\,m^{-2}$
Π_0 osmotic pressure of ions in the bulk, $N\,m^{-2}$
ρ_p particle density, $kg\,m^{-3}$
σ_0 surface density of charge, $C\,m^{-2}$
ϕ volume fraction of particles $(=1-\varepsilon)$, dimensionless
ω_i characteristic frequency of electromagnetic radiation, $rad\,s^{-1}$
ψ electrostatic potential, V
Ψ reduced electrostatic potential $[=ze\psi/(kT)]$, dimensionless

Subscripts

a apparent
A attractive
av average
c conduction
C cake
D disjoining
ent entropic
hyd hydration, or hydraulic
lim limit
L hydraulic
m membrane
T total
ξ zeta-potential
0 surface
1 solute
3 solvent
+ positive
− negative

Superscripts

0 bulk

REFERENCES

Acton, F. S., 1970, *Numerical Methods that Work*. Harper & Row, New York.

Altena, F. W. and Belfort, G., 1984, Lateral migration of spherical particles in porous flow channels: application to membrane filtration. *Chem. Engng Sci.* **39**, 343–355.

Bell, G. M. and Levine, S., 1957, Statistical thermodynamics of concentrated colloidal solutions: 1. Free energy of electrical double layers. *Trans. Faraday Soc.* **53**, 143–158.

Bell, G. M., Levine, S. and McCartney, L. N., 1970, Approximate methods of determining the double-layer free energy of interaction between two charged colloidal spheres. *J. Colloid Interface Sci.* **33**, 335–359.

Benzing, D. W. and Russel, W. B., 1981, The viscoelastic properties of ordered latices: Experiments. *J. Colloid Interface Sci.* **83**, 178–190.

Beunen, J. A. and White, L. R., 1981, The order–disorder transition in latex dispersions. *Colloids and Surf.* **3**, 371–391.

Blake, N. J., Cumming, I. W. and Streat, M., 1990, Prediction of steady state crossflow filtration using a force balance model, in *Proceedings of the Vth World Filtration Congress*. Nice, France, pp. 579–585.

Bowen, W. R. and Jenner, F., 1995a, Theoretical description of membrane filtration of colloids and fine particles: an assessment and review. *Adv. Colloid Interface Sci.* (in press).

Bowen, W. R. and Jenner, F., 1995b, The calculation of dispersion forces for engineering applications. *Adv. Colloid Intreface Sci.* (in press).

Bowen, W. R. and Jenner, F., 1995c, Electroviscous effects in charged capillaries and packed beds *J. Colloid Interface Sci.* (in press).

Carman, P. C., 1938, Fundamental principles of industrial filtration. *Trans. Instn chem. Engng* **16**, 168–188.

Carnahan, N. F. and Starling, K. E., 1969, Equation of state for nonattracting rigid spheres. *J. chem. Phys.* **51**, 635–636.

Chan, D. Y. C. and Mitchell, D. J., 1983, The free energy of an electrical double layer. *J. Colloid Interface Sci.* **95**, 193–197.

Chan, D. Y. C., Pashley, R. M. and White, L. R., 1980, A single algorithm for the calculation of the electrostatic repulsion between identical surfaces in electrolyte. *J. Colloid Interface Sci.* **77**, 283–285.

Chen, C. S. and Levine, S., 1972, Double layer interaction energy of a concentrated system of charged parallel colloidal plates in aqueous electrolyte. *J. chem. Soc. Faraday Trans.* II **68**, 1497–1513.

Cohen, J. A., Scales, D. J., Ou-Jang, H. D. and Chaikin, P. M., 1993, Freeze-fracture electron microscopy of polystyrene colloidal crystals. *J. Colloid Interface Sci.* **156**, 137–142.

Davis, R. H. and Birdsell, S. A., 1987, Hydrodynamic model and experiments for crossflow microfiltration. *Chem. Engng Commun.* **49**, 217–234.

Derjaguin, B. V. and Landau, L., 1941, Theory of the stability of strongly charged lyophobic sols and of the adhesion of strongly charged particles in solutions of electrolytes. *Acta Physiochimica U.R.S.S.* **14**, 633–662.

Derjaguin, B. V., Voropayeva, T. N., Kabanov, B. N. and Titiyevskaya, A. S., 1964, Surface forces and the stability of colloids and disperse systems. *J. Colloid Interface Sci.* **19**, 113–135.

Doshi, M. R. and Trettin, D. R., 1981, Ultrafiltration of colloidal dispersions and macromolecular solutions in an unstirred batch cell. *Ind. Engng Chem. Fundam.* **20**, 221–229.

Ducker, W. A., Senden, T. J. and Pashley, R. M., 1992, Measurement of forces in liquids using a force microscope. *Langmuir* **8**, 1831–1836.

Dzyaloshinskii, I. E., Lifshitz, E. M. and Pitaevskii, L. P., 1961, The general theory of van der Waals forces. *Adv. Phys.* **10**, 165–209.

Evans, R. and Napper, D. H., 1978, Disjoining pressures in colloidal dispersions. *J. Colloid Interface Sci.* **63**, 43–48.

Fane, A. G., 1986, Ultrafiltration: factors influencing flux and rejection, in, *Progress in Filtration and Separation* (Edited

by R. J. Wakeman) Vol. 4, pp. 101–179. Elsevier, Amsterdam.

Fane, A. G., Fell, C. J. D. and Nor, M. T., 1982, Ultrafiltration in the presence of suspended matter. *Ind. chem. Engng Jubilee Symp.* **73**, C1–12.

Feat, G. R. and Levine, S., 1974, Double layer interaction of two charged colloidal spherical particles of a concentrated dispersion in a medium of low dielectric constant. Part 2 — a cell model *J. chem. Soc. Faraday Trans. II* **71**, 102–118.

Field, R. W., 1993, Transport processes in membrane systems, in *Membranes in Bioprocessing: Theory and Applications* (Edited by J. A. Howell, V. Sanchez and R. W. Field) pp. 55–112. Chapman and Hall, London.

Grabbe, A. and Horn, R. G., 1993, Double-layer and hydration forces measured between silica sheets subjected to various surface treatments. *J. Colloid Interface Sci.* **157**, 375–383.

Guldbrand, L., Nilsson, L. G. and Nordenskiöld, L., 1986, A Monte Carlo simulation study of electrostatic forces between hexogonally packed DNA double helices. *J. chem. Phys.* **85**, 6687–6698.

Hachisu, S., Kobayashi, Y. and Kose, A., 1973, Phase separation in monodisperse latices. *J. Colloid Interface Sci.* **42**, 342–348.

Hall, K. R., 1972, Another hard-sphere equation of state. *J. chem. Phys.* **57**, 2252–2254.

Hamaker, H. C., 1937, London–van der Waals attraction between spherical particles. *Physica* **4**, 1058–1072.

Happel, J., 1958, Viscous flow in multiparticle systems: slow motion of fluids relative to beds of spherical particles. *A.I.Ch.E. J.* **4**, 197–201.

Happel, J. and Brenner, H., 1973, *Low Reynolds Number Hydrodynamics*. Kluver, The Netherlands.

Hiltner, P. A. and Krieger, I. M., 1969, Diffraction of light by ordered suspensions. *J. phys. Chem.* **73**, 2386–2389.

Horn, R. G. and Israelachvili, J. N., 1981, Measurement of structural forces between two particles in a nonpolar liquid. *J. chem. Phys.* **75**, 1400–1411.

Hoskin, N. E. and Levine, S., 1956, The interaction of two identical spherical colloidal particles: II. The free energy. *Phil. Trans. R. Soc. Lond.* **A248**, 449–466.

Hough, D. B. and White, L. R., 1980, The calculation of Hamaker constants from Lifshitz theory with applications to wetting phenomena. *Adv. Colloid Interface Sci.* **14**, 8–41.

Hunter, R. J., 1985, *Foundations of Colloid Science, Vol.* 1. Oxford University Press, Oxford.

Hunter, R. J., 1981, *Zeta Potential in Colloid Science*. Academic Press, London.

Iler, R. K., 1979, *Chemistry of Silica*. Wiley-Interscience, New York.

Israelachvili, J. N., 1991, *Intermolecular and Surface Forces* 2nd Edition. Academic Press, London.

Kose, A., Ozaki, M., Takano, K., Kobayaski, Y. and Hachisu, S., 1973, Direct observation of ordered latex suspension by metallurgical microscope. *J. Colloid Interface Sci.* **44**, 330–338.

Kozeny, J., 1927, Über kapillare Leitung des Wassers im Boden (Aufstieg, Versickerung und Anwendung auf die Bewässerung). *Ber. Wien. Akad.* **136a**, 271–306.

Krieger, I. M. and O'Neill, F. M., 1968, Diffraction of light by arrays of colloidal spheres. *J. Am. Chem. Soc.* **90**, 3114–3120.

Langbein, D., 1970, Retarded dispersion energy between macroscopic bodies. *Phys. Rev. B* **2**, 3371–3383.

Le, M. S. and Howell, J. A., 1984, Alternative model for ultrafiltration. *Chem. Engng Res. Des.* **62**, 373–380.

Levine, S., Marriott, J. R., Neale, G. and Epstein, N., 1975, Theory of electrokinetic flow in fine cylindrical capillaries at high zeta potentials. *J. Colloid Interface Sci.* **52**, 136–149.

Lifshitz, E. M., 1956, The theory of molecular attraction forces between solid bodies. *Sov. Phys. JETP* **2**, 73–83.

London, F., 1930, Theory and systematics of molecular forces. *Z. Physik* **63**, 245–279.

Mackley, M. R. and Sherman, N. E., 1992, Crossflow cake filtration mechanisms and kinetics. *Chem. Engng Sci.* **47**, 3067–3084.

Mahanty, J. and Ninham, B. W., 1976, *Dispersion Forces*. Academic Press, London.

Malitson, I. H., 1965, Interspecimen comparison of the refractive index of fused silica. *J. Optimization Soc. Am.* **55**, 1205–1209.

McDonogh, R. M., Fell, C. J. D. and Fane, A. G., 1989, Charge effects in the crossflow filtration of colloids and particulates. *J. Membrane Sci.* **43**, 69–85.

McDonogh, R. M., Fell, C. J. D. and Fane, A. G., 1984, Surface charge and permeability in the ultrafiltration on non-flocculating colloids. *J. Membrane Sci.* **21**, 285–294.

McDonogh, R. M., Welsch, K., Fell, C. J. D. and Fane, A. G., 1992, Incorporation of the cake pressure profiles in the calculation of the effect of particle charge on the permeability of filter cakes obtained in the filtration of colloids and particulates. *J. Membrane Sci.* **72**, 197–204.

Michaels, A. S., 1968, New separation technique for the CPI. *Chem. Engng Prog.* **64**, 31–43.

Miklavic, S. J. and Ninham, B. W., 1990, Competition for adsorption sites by hydrated ions. *J. Colloid Interface Sci.* **134**, 305–311.

Ninham, B. W. and Parsegian, V. A., 1971, Electrostatic potential between surfaces bearing ionizable groups in ionic equilibrium with physiologic saline solution. *J. theor. Biol.* **31**, 405–428.

O'Brien, R. W. and White, L. R., 1978, Electrophoretic mobility of a spherical colloidal particle. *J. chem. Soc. Faraday Trans. II* **74**, 1607–1626.

Onoda, G. Y. and Liniger, E. G., 1990, Random loose packings of uniform spheres and the dilatancy onset. *Phys. Rev. Lett.* **64**, 2727–2730.

Pailthorpe, B. A. and Russel, W. B., 1982, The retarded van der Waals interaction between spheres. *J. Colloid Interface Sci.* **89**, 563–566.

Philipse, A. P. and Pathmamanoharan, C., 1993, Liquid permeation (and sedimentation) of dense colloidal hard-sphere packings. *J. Colloid Interface Sci.* **159**, 96–107.

Prieve, D. C. and Russel, W. R., 1988, Simplified predictions of Hamaker constants from Lifshitz theory. *J. Colloid Interface Sci.* **125**, 1–13.

Reihanian, H., Robertson, C. R. and Michaels, A. S., 1983, Mechanisms of polarization and fouling of ultrafiltration membranes by proteins. *J. Membrane Sci.* **16**, 237–258.

Reiner, E. S. and Radke, C. J., 1991, Electrostatic interactions in colloidal suspensions: tests of pairwise additivity. *A.I.Ch.E. J.* **37**, 805–824.

Rice, C. L. and Whitehead, R., 1965, Electrokinetic flow in a narrow cylindrical capillary. *J. phys. Chem.* **69**, 4017–4024.

Romero, C. A. and Davis, R. H., 1988, Global model of crossflow microfiltration based on hydrodynamic particle diffusion. *J. Membrane Sci.* **39**, 157–185.

Romero, C. A. and Davis, R. H., 1990, Transient model of crossflow microfiltration. *Chem. Engng Sci.* **45**, 13–25.

Russel, W. B., 1987, *The Dynamics of Colloidal Systems*. University of Wisconsin Press, Madison.

Russel, W. B., Saville, D. A. and Schowalter, W. R., 1989, *Colloidal Dispersions*. Cambridge University Press, Cambridge.

Smoluchowski, M. von, 1918, Versuch einer mathematischen Theorie der Koagulationskinetik kolloider Lösungen. *Z. phys. Chem.* **93**, 129–168.

Stamatakis, K. and Chi Tien, 1993, A simple model of crossflow filtration based on particle adhesion. *A.I.Ch.E. J.* **39**, 1292–1302.

Strauss, M., Ring, T. A. and Bowen, H. K., 1987, Osmotic pressure and concentrated suspensions of polydisperse particles with thick double layers. *J. Colloid Interface Sci.* **118**, 326–334.

Tadros, M. E. and Mayes, I., 1980, Effects of particle properties on filtration of aqueous suspensions, in *Fine Particles Processing* (Edited by Sanasundaran) Vol. 2, pp. 1583–1593. Amer. Inst. Min. Met. Petr. Eng., New York.

Tiller, F. M., Crump, J. R. and Ville, F., 1980, A revised approach to the theory of cake filtration, in *Fine Particles Processing* (Edited by Sanasundaram) Vol. 2, pp. 1549–1582. Amer. Inst. Min. Met. Petr. Eng., New York.

Verwey, E. J. W. and Overbeek, J. Th. G., 1948, *Theory of the Stability of Lyophobic Colloids*. Elsevier, Amsterdam.

Vilker, V. L., Colton, C. K. and Smith, K. A., 1981, Concentration polarization in protein ultrafiltration. *A.I.Ch.E. J.* **27**, 637–645.

Wakeman, R. J. and Tarleton, E. S., 1991, Colloidal fouling of microfiltration membranes during the treatment of aqueous feed streams. *Desalination* **83**, 35–52.

Wigner, E. and Seitz, F., 1933, On the constitution of metallic sodium. *Phys. Rev.* **43**, 804–810.

Wijmans, J. G., Nakao, S. and Smolders, C. A., 1984, Flux limitation in ultrafiltration: osmotic pressure model and gel-layer model. *J. Membrane Sci.* **20**, 115–124.

Wijmans, J. G., Nakao, S., van den Berg, J. W. A., Troelstra, F. R. and Smolders, C. A., 1985, Hydrodynamic resistance of concentration polarization boundary layers in ultrafiltration. *J. Membrane Sci.* **22**, 117–135.